TÉCNICO LISBOA

Establishment of constitutive model for impact damage of plant fiber reinforced composite materials

João Carlos da Cruz Dias

Thesis to obtain the Master of Science Degree in

Aerospace Engineering

Supervisor: Prof. José Miranda Guedes

Examination Committee

Chairperson: Prof. Fernando José Parracho Lau
Supervisor: Prof. José Miranda Guedes
Member of the Committee: Prof. Maria Amélia Ramos Loja

November 2021

Dedicated to my family.

Acknowledgments

I would like to start by thanking my supervisor, Prof. José Miranda Guedes for all his support, help, guidance and infinite patience and encouragement to answer my questions and to help me with the difficulties that I've found during the my work.

I would like to acknowledge the help of Dr. Yiou Shen, whom sugested me the theme for the thesis and gave me the inicial guidance.

I am thankful for the years at Instituto Superior Técnico. For the good professors that I have had the pleasure of meeting and learn from. The friends that I've made both from Aerospace and Naval Engineering, that supported me during difficult times and made everything more fun. The co-workers that became friends which taught me a lot about responsibility and accountability.

To my dearest Joana: without you I wouldn't have endured, worked hard and finished this work. I thank you for all the support you have given me even when knowing that all you could do was cheer me, you were relentless in making me smile and picking me up by being the caring, wonderful and loving person that you are.

At last, to my parents: It has been a long journey and you were always supportive through it all. Even at the biggest costs for you, you were always unconditionally supportive and always did your best to help and give me the opportunities that a son from a woodworker and a cleaning lady could only ever dream of. I am, and will eternally be, thankful to both of you.

Resumo

Com a crescente utilização de materiais compósitos na indústria aeroespacial e a também crescente necessidade de aumentar a eficiência e baixar a pegada de carbono desta indústria, compósitos verdes (ou compósitos reforçados por fibras de origem natural) apresentam-se como uma boa alternativa para manufatura de alguns painéis internos de aeronaves pois permitem baixar o peso (e possivelmente alguns custos) destas. As superfícies sujeitas a impacto (revestimentos de lavabos e compartimentos de carga de cabine) são uma possivel aplicação e, desta forma, o estudo de impactos a baixas velocidades em compósitos reforçados por fibras naturais é importante.

O desenvolvimento de um modelo constitutivo para impacto a baixa velocidade que considere o comportamento não linear das fibras naturais, causado pelo enrolamento destas de forma a criar fios, permite um melhor estudo numérico destes materiais.

O modelo desenvolvido é capaz de considerar o comportamento não linear dos fios, introduzindo-o no critério de falha de Hashin, através de premissas propostas na literatura. Foi possivel usar o critério de falha para um caso em que a carga não está alinhada com o eixo das fibras, de acordo com o modelo de Hashin, modficando-o de forma a que fosse incluido o efeito do ângulo de enrolamento do fio. Com isto, foi possivel fazer uma análise numérica do problema recorrendo a uma sub-rotina VUMAT e ao programa Abaqus/Explicit.

Foi feita uma análise do impacto a baixa velocidade num compósito laminado unidirecional de dezasseis camadas para cinco valores de velocidade de impacto (correspondentes a $5J$, $7J$, $8J$, $9J$ e $10J$) e os resultados obtidos foram analisados. São também apresentadas conclusões, principais feitos alcançados e trabalhos futuros.

Palavras-chave: Materiais Compósitos Laminados, Fibras Naturais, Ângulo de Enrolamento, Impacto de Baixa Velocidade, Comportamento Não Linear.

Abstract

Considering the increasing use of composite materials in the aerospace industry and the growing necessity to obtain greater efficiency and lowering its carbon footprint, green composites (or natural fiber reinforced composites) presents a good alternative for for the manufacturing of some internal panels by reducing the weight, and possibly do the cost, of the plane in general. Areas susceptible to impact (lavatories and over-head cargo space linings) are possible applications and, as such, the study of low velocity impact on plant fiber reinforced composites is important.

The development of a constitutive model for low velocity impact that considers the nonlinear behaviour of natural fibers, caused by them being normally used after twisted together into a yarn, allows for a better numerical study of these materials.

The model developed, obtained considering literature based assumptions, is able to consider the yarn nonlinear behaviour by introducing it into the Hashin failure criteria. It was possible to use the failure criteria for an off-axis loading case presented by Hashin modifying it to take the twist angle of the reinforcing yarns into consideration. Thus, it is possible to numerically analyse the problem with the development of a VUMAT subroutine and the Abaqus/Explicit solver.

The low velocity impact analysis was made for a sixteen layer unidirectional composite laminate under five different impact velocity cases (correspondent to $5J$, $7J$, $8J$, $9J$ and $10J$) and the results are presented and analysed. Conclusions about the work done, achievements and future work are also presented.

Keywords: Laminated Composite Materials, Natural Fiber, Twist Angle, Low Velocity Impact, Nonlinear behaviour.

Contents

List of Tables

List of Figures

Nomenclature

Greek symbols

α	Twist angle.
ϵ	Normal strain.
ϵ^0	Strain in reference configuration.
η_l	Fiber density distribution.
η_l	Fiber length distribution.
Γ	Fracture energy.
γ	Shear strain.
ν	Poisson's Ratio.
ρ	Density.
σ	Normal stress.
σ^0	Stress in reference configuration.
σ_α	Ultimate stress considering twist angle.
σ_θ	Stress in off-axis loading case.
τ	Shear stress.
θ	Fiber orientation angle.

Roman symbols

C	Stiffness matrix.
D	Diameter.
d	Damage.
E	Elasticity modulus.
$E_{absorbed}$	Absorbed energy.

$E_{initial}$ Initial energy.

$E_{kinetic}$ Kinetic energy.

G Shear modulus.

I Stress Invariants.

L Length of one turn of a yarn.

l Unsupported length.

m Mass.

r Fiber radius.

S Compliance matrix.

S_m Matrix shear stiffness control parameter.

T Twist level.

t Thickness.

V Volume.

v Impact velocity.

w Width.

x_1, x_2, x_3 Cartesian coordinate system for the material.

Subscripts

0 Fiber in the zero degree direction.

$1, 2, 3$ Material Cartesian components.

90 Fiber in the ninety degree direction.

A Referent to the composite axial direction.

c Compressive case.

f Referent to the fiber.

i, j, k, l Matrix index referring to the material Cartesian direction.

m Referent to the matrix.

T Referent to the composite transverse direction.

t Tensile case.

u Ultimate.

v Hollow (referring to volume fraction).

Superscripts

$+$ Tensile case.

$-$ Compressive case.

i Inter-laminar.

d Deformed.

Chapter 1

Introduction

1.1 Motivation and topic overview

Composite materials are a type of materials widely used for various engineering applications. Some examples of the industries that use this type of materials are the automotive, the naval and the aerospace. Composite materials are a mixture of two or more materials that specifically combined in order to produce a final material with a desired set of properties. This work will focus on the fiber reinforced laminated composite materials, which consist on the stacking of layers of a matrix reinforced with fibers. These fibers have a high strength and high modulus that allow for obtaining a reinforced material.

The combination of materials permits the conception of a material which will have the properties that are the most fit for a specific application. The aerospace industry utilizes these as it is possible to obtain a material that has a high strength, high impact energy, good fatigue performance, good corrosion resistance and high fracture toughness, while maintaining a low weight. [1]

In aerospace, using materials that offer a desirable set of properties but that save on the weight of the vehicle has major benefits since it provides a more efficient flight and achieves a more environmentally friendly solution. As an illustrative example, the type of materials used in the Airbus A350 and their quantity in the form of percentage are featured on Figure 1.1 where its possible to observe that the most used type of materials are the composites.

As one of the main challenges on aviation nowadays is to reduce the environmental impact, it is beneficial to make the composite materials more ecological using natural fibers as a reinforcement. They have a degradable nature, their sourcing accounts for lower carbon emissions and their production is more energy efficient [4, 5]. These also have mechanical properties, in some cases, similar to glass fibers [6] and they are light-weight due to their low density [7]. This light-weight property makes them an ideal substitute for the use in internal panels (from flooring to lavatories or cargo hold linings) since they can reduce the weight of these components and greatly improve the efficiency of the aircraft by lowering the weight of the aircraft which improves the range, fuel consumption and carbon emissions [8]. All of this allows for the possibility of replacing the use of synthetic fibers by natural ones as the reinforcement for composite materials in certain applications, like over head cargo hold or lavatory linings that are

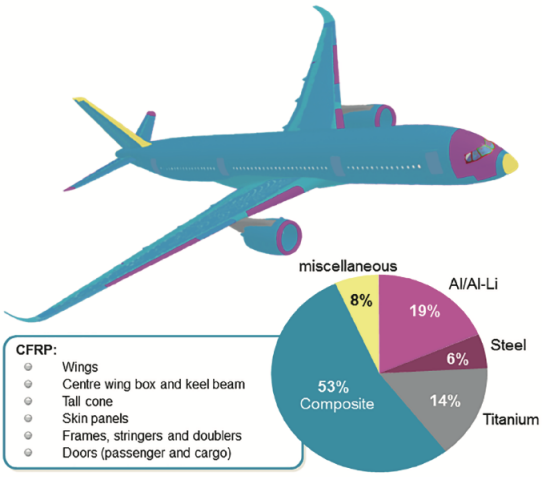

Figure 1.1: Different materials in quantities on Airbus A350 [2, 3]

subjected to impacts of lower velocities which implies a study of it's properties and behaviour.

1.1.1 Natural Fiber Reinforced Composites

Natural fibers have a wide selection of sources and, as can be observed in Figure 1.2, they can be divided into three main groups. This work will focus on the non-wood plant fibers designated as "bast". From these type of fibers, the ones with the biggest focus on this project will be: flax, sisal and hemp. The constitution and structure of these types of fibers is identical and, in order to simplify, only the flax fiber will be explained in detail.

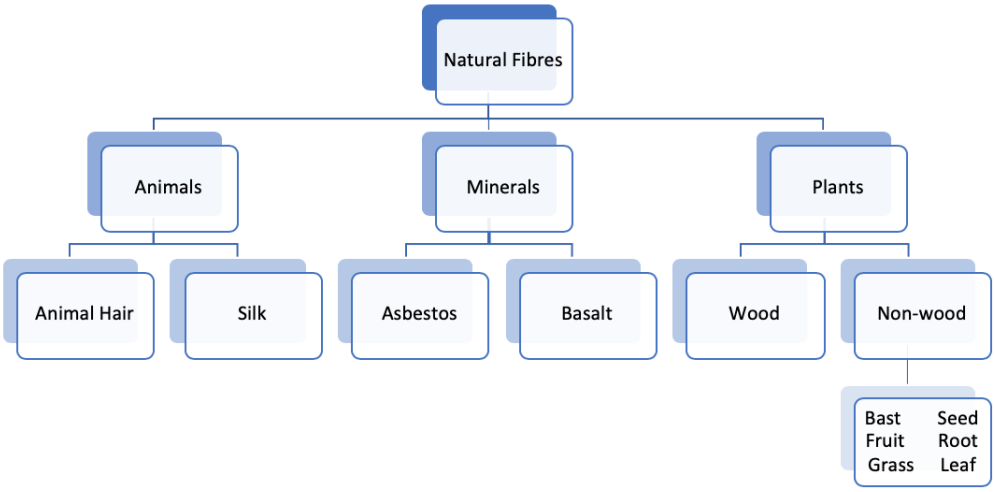

Figure 1.2: Types of natural fibers diagram

Constitution of flax fibers

In Figure 1.3 a) and b) is possible to observe a microscopic image of flax fiber and to conclude that the fibers have a non-cylindrical shape as well as a variable diameter along its length. In the last picture,

d), is possible to see the cross-section of the stem and the different constituents present on it. These parts of the stem are (from the outside and inwards) bark, phloem, xylem and a central void. The fibers are present on the stem in agglomerates and are maintained together by pectin, a glue-like substance. In c) is possible to observe an agglomerate of fibers (marked on red) and it is also possible to identify some regions on each fiber. The fiber itself can be divided into three parts, namely: the Primary Wall, the Secondary Wall and the Lume, as seen in Figure 1.4. The Primary Wall is mainly made of cellulose microfibrils within a network of hemicellulose, pectin compounds, and glycoproteins [9, 10]. The Secondary Wall is the biggest component of the fiber and can also be subdivided further into the S1, S2 and S3 layers, also seen in the Figure 1.4. These three layers vary in composition and thickness, with the S2 being the thickest of all, constituting approximately 70 % to 80 % of the fiber weight, making this the layer that will gran the mechanical properties to the fiber. These layers are composed of hemicellulose, lignin and cellulose with this last one being the one with the biggest presence and impact on fiber properties. [9, 10]

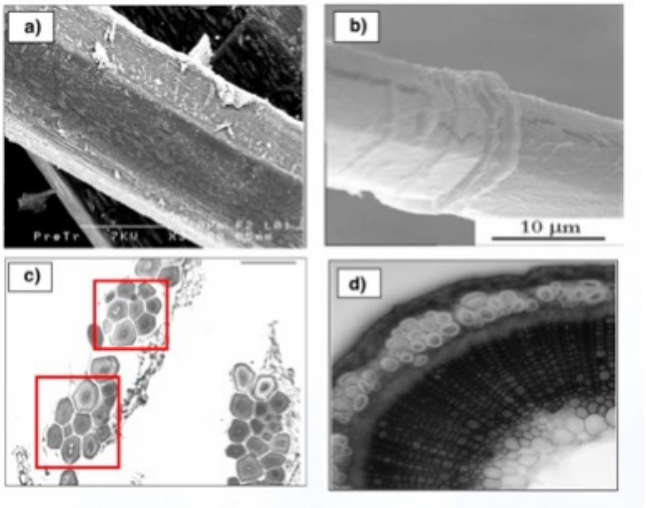

Figure 1.3: Microscopic images of flax fibers. [Courtesy of School of Aerospace Engineering at Tongji University]

Flax fibers are composed by cellulose, hemicelulose, lignin, pectin and wax/fat, being cellulose the one that has more quantity present and wax/fat only residual in presence. Since cellulose is the main component in the flax fibers, it is agreed that the main properties of the fibers, like stiffness or strength, come from this component. Cellulose is a long polymer constituted by glucose molecules. Cellulose is in turn, connected into microfibrils, whose number of chains of cellulose can be between 30 and 100. For this, the higher cellulose content present on a fiber, the more economically viable it is to produce and use these materials. [10]

1.1.2 Low-velocity impact

Another concept that is important and worth introducing and reviewing is the low-velocity impact. Sjöblom *et al.* [13] and Shivakumar *et al.* [14] defined the low-velocity impact as events that can be considered as quasi-static events with velocities of small order they also defined it as varying according to the target (stiffness and material properties) and impactor (mass and stiffness). For low-velocity impact,

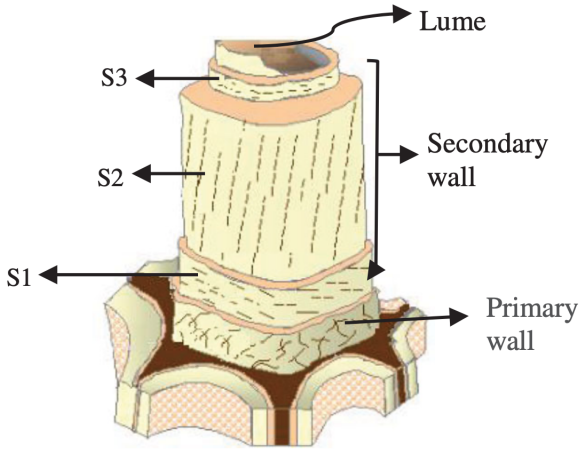

Figure 1.4: Representation of the constitution of flax fibers. [11, 12]

the target's dynamic structural response has very important role since the contact duration is long enough to allow the entire structure to respond to the impact and, as a consequence, more energy is absorbed elastically.

Considering the general techniques employed for the simulation of impact (drop weight, Charpy, Izod, etc), Cantwell and Morton [15] defined the low-velocity as up to $10(m.s^{-1})$. Abrate [16], in his review, stated that the impacts up to $10(m.s^{-1})$ could be considered as low-velocity.

Another form of classification, that was considered by Liu and Malvern [17] and Joshi and Sun [18], is by the damage incurred, especially if the damage is the principal concern, as it's the case on the present work, with low-velocity being characterized by the delamination and matrix cracking.

It's also important to refer the work by Davies and Robinson [19, 20] in which the low-velocity impact is defined as the stress wave through-thickness playing no significant part in the stress distribution and sugest a simple model to give the transition to high velocity. For this, a cylindrical zone, under the impactor, is considered to have a uniform strain and stress wave propagating through the plate, giving the compressive strain as [19]:

$$\varepsilon = \frac{\text{impact velocity}}{\text{speed of sound in the material}} \tag{1.1}$$

For epoxy composites and for failure strains between 0.5% and 1% this gives the transition to stress wave dominated events at $10 - 20(m.s^{-1})$.

1.2 Objectives

The present work proposes the development of a constitutive model and consequent numerical implementation and validation that can successfully predict the behaviour of unidirectional natural fiber reinforced composite materials under a low-velocity impact. This work will also make it possible to understand the mechanical behaviour of natural fiber reinforced composites, low-velocity impact and it's consequences, the nonlinearity causes and changes on the study of materials, as well as the difficulties inherent to it.

It is important to achieve a model that allows for the numerical simulation of the proposed problem and for a good prediction of the behaviour of the studied material. Computational work, opposed to experimental work, has a lower cost of materials, manufacturing and time. It enables the study of materials and it's applications in an easier and cheaper way and, consequently, allows for a more accessible study and implementation of these materials.

1.3 Thesis Outline

As for the organisation of the present document, it can be outlined as follows:

- Chapter 1 - Introduction
  - In this chapter, a small introduction for the topic and motivation is made, as well as the work's objective and the outline.
- Chapter 2 - Background
  - In this chapter the background of the work developed is presented. Natural fibers and their usage for the reinforcement of composite materials are explained as well as the non-linearity observed in materials with these fibers as a reinforcement. After this, the low velocity impact and the typical material behaviour are explained. It is also shown the different models for the impact evaluation and failure that were studied.
- Chapter 3 - Implementation
  - In this chapter, the constitutive model is presented as well as the numerical implementation and validation methods.
- Chapter 4 - Numerical Implementation
  - The numerical implementation and how it was achieved is presented in this chapter from the modelling of the composite to the simulation and numerical analysis.
- Chapter 5 - Results
  - The results obtained from the computational implementation of the models considered on Chapter 3, obtained using the methodology explained in Chapter 4, are presented and validated.
- Chapter 6 - Conclusions
  - In this chapter the conclusions about the work done, achievements and future work are presented.

Chapter 2

Background

2.1 Laminated Composite Materials

Composite materials are a combination of two or more materials that, when combined, can achieve mechanical properties which would not be able to be observed on the raw materials by themselves. Fiber reinforced composite materials are a kind of composite material where fibers are used as a reinforcement embedded into a matrix. For example, fibers with higher strength and higher modulus can be reinforcing a matrix. Reddy [21] states that fibers are stiffer and stronger than the same original material due to having geometrically, a near crystal-sized diameter and a very high length-to-diameter ratio. It is also stated on his work that short fibers paradoxically exhibit better structural properties than the long fibers. The matrix has the same characteristics as their own bulk material [21].

Laminated composite materials are obtained by the stacking of plies (layers) of a composite material (usually composed by a matrix reinforced by fibers). These plies are commonly composed of fibers aligned in a single or dual direction and, in the stacking process, plies with fibers aligned in different directions can be used in order to achieve a different set of mechanical properties.

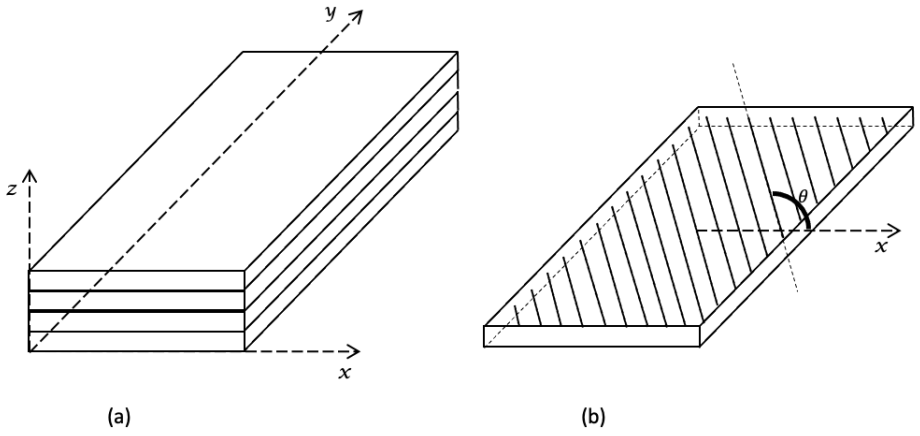

Figure 2.1: Laminated composites (a) stacking scheme and (b) fibers in-ply orientation

For the case at study, the composite will be reinforced by unidirectional fibers and, in order to simplify

the calculations will be considered as being oriented such as $\theta = 0$ making it so that the load is applied in-axis.

In these materials, the strength and stiffness are given by the fibers and the matrix is used to keep these fibers together, preventing them for being exposed to the environment surrounding and allowing for the dispersion of the applied stresses through the different fibers. Matrices and fibers can be of various origins and some examples of fibers are carbon, flax, glass, sisal, aluminium, etc. Some examples of matrices are polymeric resins (epoxy or polyester) and can also be metallic or ceramic. [22] [23]

2.1.1 Matrix

While the matrix materials used on the composite materials can be of various origins, the focus on this work will be set on the polymeric matrices.

The resins can be of two main types, being them thermosets or thermoplastics. The main difference between these materials is that the thermoset materials can be strengthened by heating but can not be heated or remoulded after the initial forming while the thermoplastics can be reheated, remolded and cooled without changing it's properties. Thermoset resins have the advantage of good impregnation of the fibers due to their low viscosity at liquid state. At Table 2.1 it's possible to observe the differences between some of the used types of thermoset polymers used.

Type of resin	Density (g/cm^3)	Elasticity Modulus (GPa)	Tensile Strength (MPa)	Elongation at failure (%)	Vitreous transition temperature ($^\circ C$)
Epoxy	1,2 - 1,3	2,0 - 4,0	60 - 80	1,0 - 8,0	100 - 270
Unsaturated Poliester	1,0 - 1,25	3,6	30 - 50	1,8 - 2,5	260
Phenolic	1,2 - 1,3	2,0 - 3,0	20 - 70	1,0 - 5,0	70- 120
Vinyl	1,12 - 1,16	3,5	68 - 82	3,0 - 4,0	102 - 150

Table 2.1: Properties of some thermoset polymeric matrixes. [24]

2.1.2 Reinforcing fibers

As stated, the reinforcing fibers can have different sources and can be natural or synthetic with very different sets of properties. The most widely used are from a synthetic nature, like carbon and glass fibers. A growing trend, nowadays, is for the usage of fibers from natural sources, mainly plants. [4, 25]

As it is possible to gather from Figures 2.2, 2.3 and 1.4, the natural fibers are a complex resource that can be regarded as a composite material by themselves.

From Figures 2.3 and 1.3 it is possible to point some facts about the plant fibers that illustrate the complexity of these materials. The cross-section of the fibers is a polygon that can be viewed as a circle, in order to allow for the simplification of their study. A problem with the transversal cross-section is that the diameter of the fiber through it's length is not constant. Another important remark is about the microfibrils and their angle with the axis of the plant. McLaughlin et al. [27] found that the angle that the microfibril had, in respect to the fiber central axis, would change the material properties that would be modelled with a variation of the $\cos^2(\alpha)$. It is also possible to observe that the fibers have an hollow part (also seen named as Lumen in Figure 1.4). The hollow centre of the natural fibers, their high

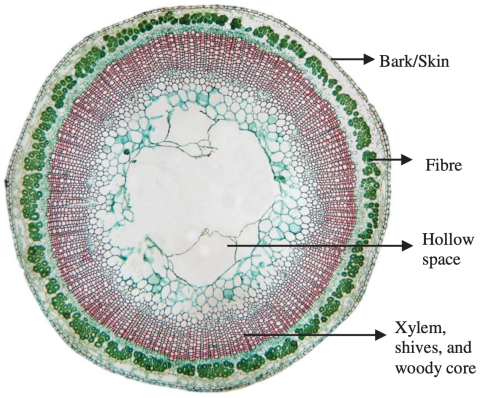

Figure 2.2: Stem cross section composition. [26]

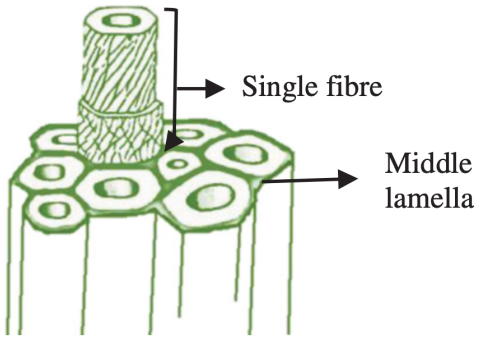

Figure 2.3: Fiber agglomerate organisation. [26]

susceptability to temperature and moisture fluctuations and the yarn twist angle (when the fibers are bundled together into yarns) generate nonlinear behaviours. Models for this behaviour will be introduced on Subsection 2.2.

For the simplification of the problem, the work to be done from now on will consider that the the diameter of the fibers is constant and the influence of the hollow center and the microfibril alignment will be disregarded due to the dimensions and scaling of the problem, meaning that the author decided, after careful consideration and consultation, that the scale of the dimensions of the composite material to be studied would mitigate the influence of the aforementioned simplifications. These simplifications can also be observed on the work by Shah et al. [28] taken from Hearle [29] that will be used ahead for the creation of the mathematical model.

Natural fibers vs glass fibers

In this subsection it is possible to observe the comparison between plant and glass fibers, in order to explain why are these fibers a viable alternative to the use of the traditional synthetic fibers, namely the glass fibers as matrix reinforcement for the creation of composite materials.

On Table 2.2, the comparison between some natural fibers (flax, hemp, jute and sisal) are compared with the most common glass fiber, E-glass. The choice for fiber to use has a strong geographical correlation, being that Europe has a bigger focus on flax fibers whereas China uses more fibers like hemp, jute and sisal [30].

Fibra	Density (g/cm^3)	Length (mm)	Failure Strain (%)	Tensile strenght (MPa)	Young's Modulus (GPa)	Specific tensile strength (MPa/gcm^{-3})	Specific Yong's modulus (MPa/gcm^{-3})
Flax	1.5	5 - 900	1.2 - 3.2	354 - 1830	27 - 80	230 - 1220	18 - 53
Hemp	1.5	5 - 55	1.6	550 - 1110	58 - 70	370 - 740	39 - 47
Jute	1.3 - 1.5	1.5 - 120	1.5 - 1.8	393 - 800	10 - 55	300 - 610	7.1 - 39
Sisal	1.3 - 1.5	900	2.0 - 2.5	507 - 855	9.4 - 28	362 - 610	6.7 - 20
E-glas	2.5	Continuous	2.5	2000 - 3000	70	800 - 1400	29

Table 2.2: Comparison between natural fibers and E-glass. [30]

On a practical view, the glass and natural fibers have some advantages and disadvantages. Considering the possibility of some natural fibers having mechanical properties close to the ones observed in the glass

fibers, creating the flexibility of using the natural fiber with the best properties for a specific application, there are three important considerations to make:

1. **Weight** From Table 2.2, it's possible to observe that the natural fibers have a lower density when compared to the glass fibers. This, combined with the flexibility for the mechanical properties, makes the natural fibers an appealing alternative to the glass fiber composites for applications that are sensible to the weight.

2. **Sensitivity** Shen, *et al.* [31] studied the effect of temperature and moisture absorption on natural fiber reinforced composites and found that when compared with their glass counterparts, natural fibers are more susceptible to both environment temperature and moist content during the manufacturing process of the composite material as well as in the composite application environment.

3. **Health** The glass fibers, depending of their size, have different levels of harmful effects on the human body with biggest impact to the respiratory tract [32]. For the time being, harmful effects for the natural fibers have yet to be identified.

Following the statement that the mechanical properties of a composite reinforced with natural fibers can be different and more adequate to a specific application and it is important to considerate these three points for a better use of these materials. The fact that the natural fibers allow for the manufacturing of composites with a lower weight grants for a broader spectrum of applications. Since they are healthier, allows for a more safe environment when used for applications where the material has a lot of contact with the human body and, in the manufacturing, allows for a safer work environment when manipulating the material. The influences of temperature and humidity obliges to a consideration of the application environment, in order to make the decision about the feasibility of the implementation of these natural fiber reinforced composite materials.

Fiber Configuration

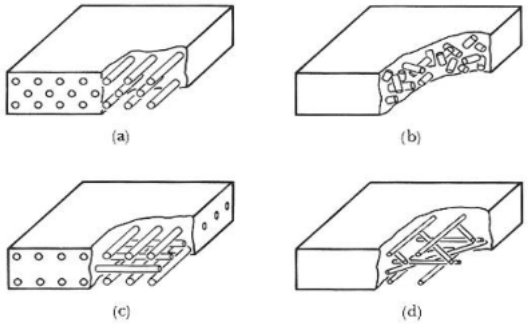

Figure 2.4: Different types of fiber orientation in composites: a) unidirectional; b) random; c) bidirectional (also woven); and d) multidirectional for different planes [33]

Natural fibers, as well as their synthetic counterparts can present various configurations when reinforcing a composite.

The problem being studied in the present work is correspondent to the Figure 2.4 (a) where is possible to observe the unidirectional configuration of the fibers that are aligned in a single direction.

2.1.3 Lamina

For this section, Reddy's [21] considerations that the lamina is 1 - a continuum (meaning that there are no voids making it in agreement with a macromechanical approach) and 2 - a linear elastic material (implicating a valid general application of the Hooke's law) are taken into account.

Anisotropy

Materials are characterized by their behaviour in what is called their constitutive formulations. Considering a purely elastic material, its constitutive formulation is a function of the state of deformation. For a case of linear elasticity this is the linear relation between stresses and strains. This relation is know as the generalized Hooke's law and is as follows:

$$\sigma_{ij} = \frac{\partial U_0}{\partial \epsilon_{ij}} = C_{ijkl}\epsilon_{kl} + \sigma^0_{ij} \tag{2.1}$$

Using the *Voigt-Kelvin notation* for the single subscript notation for stresses and strains renders the stresses $\sigma_{ij} \rightarrow \sigma_i$, the strains $\epsilon_{ij} \rightarrow \epsilon_i$ and two-subscript component $C_{ijkl} \rightarrow C_{ij}$ into non-tensor components and the Equation 2.1 becomes:

$$\sigma_i = C_{ij}\epsilon_j + \sigma^0_i \tag{2.2}$$

Assuming that the reference configuration is stress-free, $\sigma^0_i = 0$ and strain free $\epsilon^0_i = 0$, we have:

$$\sigma_i = C_{ij}\epsilon_j \tag{2.3}$$

where, σ_{ij} (σ_i) are the stress components, ϵ_{ij} (ϵ_j) are the strain components and C_{ij} are the material coefficients or stiffness tensor. All referring to an orthogonal Cartesian coordinate system (x_1, x_2, x_3 seen in Figure 2.5).

In matrix form:

$$\begin{bmatrix} \sigma_1 \\ \sigma_2 \\ \sigma_3 \\ \sigma_4 \\ \sigma_5 \\ \sigma_6 \end{bmatrix} = \begin{bmatrix} C_{11} & C_{12} & C_{13} & C_{14} & C_{15} & C_{16} \\ C_{21} & C_{22} & C_{23} & C_{24} & C_{25} & C_{26} \\ C_{31} & C_{32} & C_{33} & C_{34} & C_{35} & C_{36} \\ C_{41} & C_{42} & C_{43} & C_{44} & C_{45} & C_{46} \\ C_{51} & C_{52} & C_{53} & C_{54} & C_{55} & C_{56} \\ C_{61} & C_{62} & C_{63} & C_{64} & C_{65} & C_{66} \end{bmatrix} \cdot \begin{bmatrix} \epsilon_1 \\ \epsilon_2 \\ \epsilon_3 \\ \epsilon_4 \\ \epsilon_5 \\ \epsilon_6 \end{bmatrix} \tag{2.4}$$

It's assumed that the material is hyperelastic and, as such, the coefficients C_{ij} must be symmetric (C_{ji} by virtue of this assumption.

It is also assumed that the stress-strains relations are invertible and it is, in this way, possible to obtain the formulations for the strains:

$$\epsilon_i = S_{ij}\sigma_j \tag{2.5}$$

that in matrix form is:

$$\begin{bmatrix} \epsilon_1 \\ \epsilon_2 \\ \epsilon_3 \\ \epsilon_4 \\ \epsilon_5 \\ \epsilon_6 \end{bmatrix} = \begin{bmatrix} S_{11} & S_{12} & S_{13} & S_{14} & S_{15} & S_{16} \\ S_{21} & S_{22} & S_{23} & S_{24} & S_{25} & S_{26} \\ S_{31} & S_{32} & S_{33} & S_{34} & S_{35} & S_{36} \\ S_{41} & S_{42} & S_{43} & S_{44} & S_{45} & S_{46} \\ S_{51} & S_{52} & S_{53} & S_{54} & S_{55} & S_{56} \\ S_{61} & S_{62} & S_{63} & S_{64} & S_{65} & S_{66} \end{bmatrix} \cdot \begin{bmatrix} \sigma_1 \\ \sigma_2 \\ \sigma_3 \\ \sigma_4 \\ \sigma_5 \\ \sigma_6 \end{bmatrix} \tag{2.6}$$

where S_{ij} is the compliance parameter with $[S_{ij}] = [C_{ij}]^{-1}$

Orthotropy

From Reddy [21], in order to obtain the orthotropic mechanical properties of a lamina theoretically, using a michromechanical approach, the following assumptions were made:

1. Fibers and matrix have a perfect bonding between them;
2. The fibers are parallel between themselves and are evenly distributed in the ply;
3. At the start, the matrix is in a stress-free state without voids or cracks;
4. Both matrix and fibers are isotropic and obey Hooke's law;
5. The loads applied on the fiber are either parallel or perpendicular to it's direction.

Continuing the work of last subsection, it is possible to reduce the complexity level of Equations 2.4 and 2.6 due to to the material orthotropic behaviour reducing the elastic coeficients to 9.

$$\begin{bmatrix} \epsilon_1 \\ \epsilon_2 \\ \epsilon_3 \\ \epsilon_4 \\ \epsilon_5 \\ \epsilon_6 \end{bmatrix} = \begin{bmatrix} \frac{1}{E_1} & -\frac{\nu_{21}}{E_2} & -\frac{\nu_{31}}{E_3} & 0 & 0 & 0 \\ -\frac{\nu_{12}}{E_1} & \frac{1}{E_2} & -\frac{\nu_{32}}{E_3} & 0 & 0 & 0 \\ -\frac{\nu_{13}}{E_3} & -\frac{\nu_{23}}{E_2} & \frac{1}{E_3} & 0 & 0 & 0 \\ 0 & 0 & 0 & \frac{1}{G_{23}} & 0 & 0 \\ 0 & 0 & 0 & 0 & \frac{1}{G_{13}} & 0 \\ 0 & 0 & 0 & 0 & 0 & \frac{1}{G_{12}} \end{bmatrix} \cdot \begin{bmatrix} \sigma_1 \\ \sigma_2 \\ \sigma_3 \\ \sigma_4 \\ \sigma_5 \\ \sigma_6 \end{bmatrix} \tag{2.7}$$

Using a weighted average approach for taking into consideration the fibers and matrix influence on the lamina and obtaining the longitudinal and transverse moduli (E_1 and E_2 respectively (Equation as well as the poisson's ratio ν_{12} and the shear modulus G_{12}, we have [34]:

$$E_1 = V_f \cdot E_f + V_m \cdot E_m$$
$$E_2 = E_3 = \frac{E_f \cdot E_m}{V_m \cdot E_f + V_f \cdot E_m} \tag{2.8}$$

$$\nu_{12} = \nu_{13} = V_f \cdot \nu_f + V_m \cdot \nu_m$$
$$G_{12} = G_{13} = \frac{G_f \cdot G_m}{V_m \cdot G_f + V_f \cdot G_m} \tag{2.9}$$

Where E_f = fiber's Young modulus, ν_f = fiber's poisson ratio, V_f = fiber's volume fraction and E_m = matrix's Young modulus, ν_m = matrix's poisson ratio, V_m = matrix's volume fraction. The shear moduli for the fiber (G_f) and for the matrix (G_m) are given by:

$$G_f = \frac{E_f}{2 \cdot (1 + \nu_f)}$$
$$G_f = \frac{E_m}{2 \cdot (1 + \nu_m)} \tag{2.10}$$

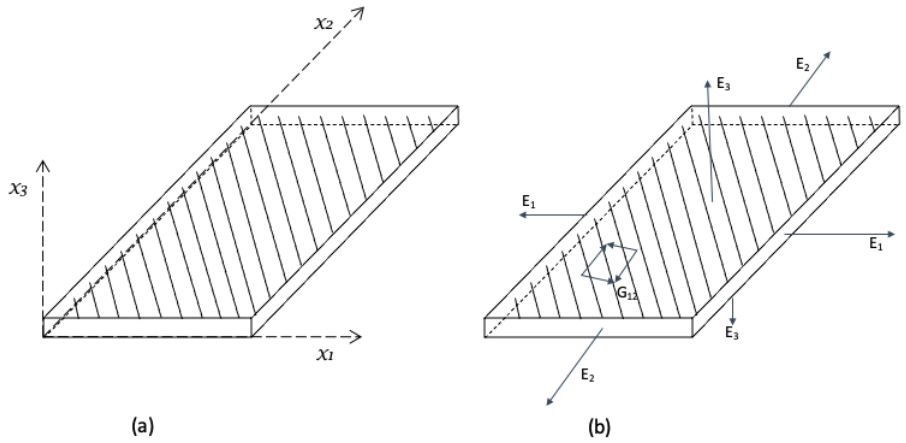

Figure 2.5: Lamina with unidirectional fiber distribution (a) planar directions x_1, x_2 and x_3 and (b) elastic constants definition for thin lamina.

2.2 Nonlinear Composite Materials

A material is considered to have a nonlinear behaviour when the relationship between stress and strain is no longer linear (as ilustrated on Figure 2.6). For the case being studied, with plant based fibers reinforcing a composite material, the nonlinearity comes from the fibers. One of the causes for the nonlinear behaviour is the moist and temperature effects on the fiber properties but, the main interest of this work is that for bigger applications of composite materials, single natural fibers (which have a limited length) cannot be used and have to be bundled into yarns. Using the yarns reinforce the composite materials, the introduction of the twist (in order to make them) creates a nonlinear behaviour. This type

of reinforcement when subjected to impact is the one that has limited research both in mathematical models and in numerical simulations.

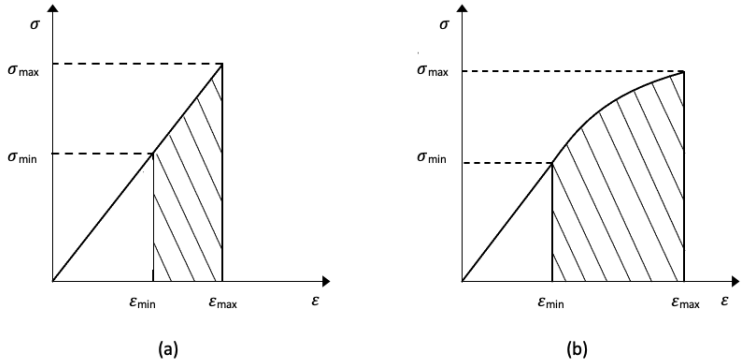

Figure 2.6: Stress-strain (a) linear and (b) nonlinear relations.

Natural Fiber Reinforced Composites

As stated before, the natural fibers can be used in composites as **simple fibers** (or *wishkers*) can be used as reinforcement for a matrix creating the composite; or **yarns**, which are the main objective of this study, are the result of the single fibers being spuned and have the benefit of being longer than the natural fibers, allowing the use of these in the production of composite materials with a much larger length and unidirectional and aligned fibers.

As was verified by Shioya *et al.* [35] during the study of the longitudinal and transverse modulus variation of continuous yarns composed of twisted natural fibers in order to comprehend the variation of this modulus with the twisting of the yarn, the result was that the larger the twisting angle, the stronger nonlinearity showing that yarns are in fact a cause of it.

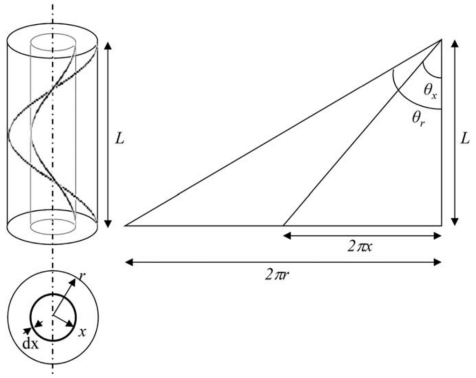

Figure 2.7: Idealized twisted fiber structure in a ring spun yarn. [36]

Yarns of natural fibers

Shah *et al.* [28] studied the possible alteration of the Tsai-Hill failure model (for uniaxial tension). For this, it was assumed that from a yarn with fibers twisted at an angle (α) it could simplified to consider it

as a cylindrical layer and after that it would be possible to "open" the impregnated yarn layer and obtain a surface with the twisted fibers as off-axis oriented fibers in the layer as shows Figure 2.8.

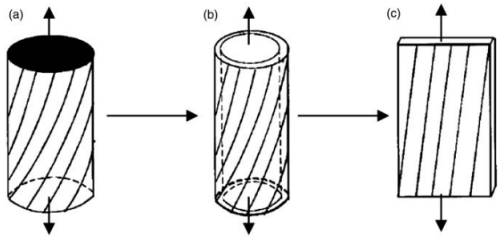

Figure 2.8: An impregnated yarn is similar to an off-axis composite. (a) twisted impregnated yarn with surface twist angle α, (b) a layer of a twisted impregnated yarn (c) the open-up structure of the layer is a laminate with off-axis loading angle θ. [28]

The Tsai-Hill failure criteria for an off-axis stress application onto a specimen, is as follows:

$$\sigma_\theta = \left[\frac{1}{\sigma_0^2}cos^4(\theta) + \left(\frac{1}{\tau^2} - \frac{1}{\sigma_0^2}\right)cos^2(\theta)sin^2(\theta) + \frac{1}{\sigma_{90}^2}sin^4(\theta)\right]^{-0.5} \tag{2.11}$$

In order to simplify the model, Shah *et al.* [28] assumed a relation between the properties as follows:

$$\frac{\sigma_0}{\sigma_{90}} = 11; \qquad \frac{\sigma_0}{\tau} = 7 \tag{2.12}$$

Obtaining a simplified equation for the model:

$$\sigma_\theta = \sigma_0\left[1 + 46 \cdot sin^2(\theta) + 74 \cdot sin^4(\theta)\right]^{-0.5} \tag{2.13}$$

The results of this representation are present in Figures 2.9 and 2.10

Since the Tsai-Hill model didn't provide the best fit, it was also studied and found that the variation of the tensile strength of the yarn can be best modelled with the quadratic variation of the cosine of the twist angle α. This can be verified through both of figures 2.9 and 2.10 that present the data from the comparison of the experimental data and different methodologies.

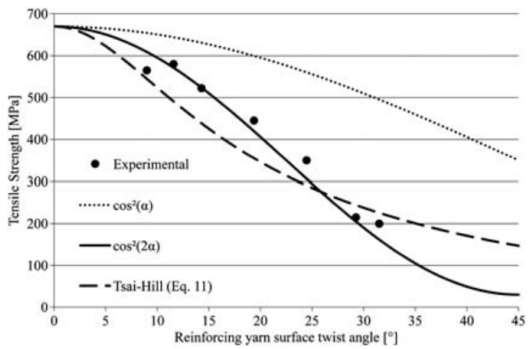

Figure 2.9: Effect of yarn twist on long flax fiber impregnated yarn. [28]

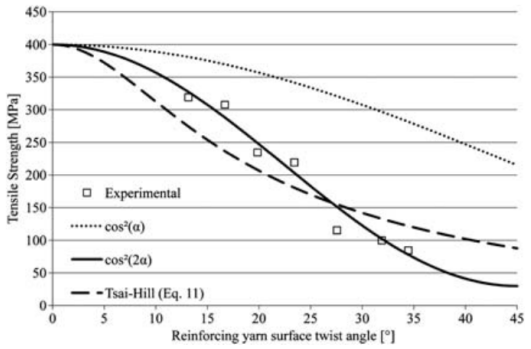

Figure 2.10: Effect of yarn twist on short flax fiber impregnated yarn. [28]

For obtaining a model that would allow for a tensile strength prediction, the approach by Shah *et al.* [28] was one of integrating the ideal structure of a staple yarn on Figure 2.7 into the Kershel efficiency factor and substituting the result into the rule of mixtures. The result of this integration and use of the rule of mixtures is present on Equation 2.14.

$$\sigma = \cos^2(2 \cdot \alpha) \cdot \eta_l \eta_d V_f \sigma_f + V_f \sigma_m)(1 - V_v)^2 \tag{2.14}$$

Where σ is the failure stress, σ_f and σ_m are the fiber failure stress and the matrix stress at fiber failure respectively. V_f is the fiber volume fraction and V_v is the "hollow" volume fraction on the composite that will be considered to be zero and, as such, $V_v = 0 \rightarrow V_m = 1 - V_f$. η_d is the density distribution on the fiber and will be considered one and η_l is the fiber length distribution (which can be considered unity for long fibers). α is the surface twist angle of the fiber and it is proposed to be $2 \cdot \alpha$ by Pan *et al.* [37] due to the yarn twisting having a dual helix configuration.

With the assumptions that fiber diameter would be constant ($\eta_d = 1$) and that the composite material contains no voids in the inside ($V_v = 0 \rightarrow V_m = 1 - V_f$). The simplified model is present on Equation 2.15.

$$\sigma_\alpha = \cos^2(2 \cdot \alpha) \cdot \eta_l V_f \sigma_f + (1 - V_f)\sigma_m \tag{2.15}$$

With this, its possible to assume that even though the modelling of the tensile behaviour of flax fibers using a $cos^2(\alpha)$ fitted to each specific experimental case, the utilization of the off-axis loading of the Tsai-Hill model, with the relatively good fit to the experimental data, allows for the possible introduction of the twist angle in a failure criteria for a general application.

2.3 Low-velocity Impact

For the last decades, the impact damage caused to a fiber reinforced laminated composite has been the subject interest and studied by various researchers. Even though a general approach is not available (mostly due to the various considerations to take into account such as temperature, humidity or, the subject of this work, non-linear behaviour) there are some theories that approach the problem based on the failure of the lamina of these types of composites.

The lamina failure criteria can be divided into two large sub-groups [38], being these the groups of criteria that allow for the consideration of the material non-homogeneity and the ones that do.

For the group of the models that don't consider the non-homogeneous behaviour of the material, we can find various valid examples such as Tsai-Wu [39], Tsai-Hill [40] or Chamis [41].

The methodologies that take into account the matrix and fiber modes of damage, take into consideration the non-homogeneous nature of the materials. These failure criteria can be further divided into two groups by either considering, or not, the interactions between plies.

If the criteria does not consider the interactions between plies, like the Maximum stress and Maximum Strain criteria, it is not considered the cross-ply relations of the stress/stains that propagate through the

lamina. For this and in order to obtain a better result for the model to experiment, the criteria considered will take into account the cross-ply stress/strain interactions.

The material behaviour is of importance to make an informed decision on what type of criteria to use and, as such, it is presented now.

Material Behaviour

For the composite materials, Richardson and Wisheart [20], in their revision, enunciated four possible failure modes for the case of these being subject to impact, being them:

1. Matrix Mode - cracking occurs parallel to the fibers due to tension, compression or shear;
2. Delamination Mode - produced by interlaminar stresses;
3. Fiber Mode - in-tension fiber breakage and in-compression fiber buckling;
4. Penetration - the impactor completely perforates the impacted surface.

The identification of the failure mode is very important since it will give information about the impact event and also the residual strength of the structure. It is also important to understand the interaction between failure modes for the understanding of the damage mode initiation and propagation. [17]

- Matrix mode

The first type of failure is the matrix damage and is induced by the transverse low-velocity impact, and usually assumes a matrix cracking form and/or the debonding between fibers and matrix [20]. Mismatching between matrix and fibers allow for the occurring of matrix cracks. In Figure 2.11 its possible to see represented the cracking and delamination pattern, as concluded by Joshi and Sun [42].

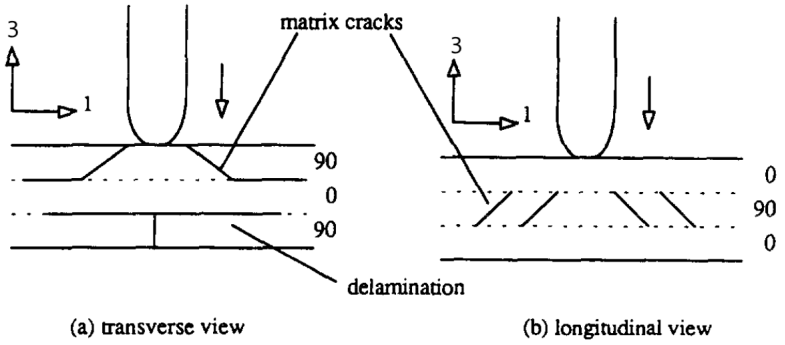

Figure 2.11: Initial damage in an impacted composite plate with 0/90/0 stacking [20, 43]

The cracks are visible in the upper layers (Figure 2.11(a)) and in the middle layer (Figure 2.11(b)) right bellow the impactor. These cracks are generated by the high shear stresses through the material and are inclined at (approximately) 45° (they can be named as *shear cracks*) and these transverse shear stresses are closely related to the contact force and area [44]. On Figure 2.11(a), the crack visible in the bottom layer is named a *bending crack* due to being generated by a high tensile bending stress and these appear, usually, in the vertical. These bending stresses are closely related to the laminate's flexural

deformation [45]. For the type of cracking that appears, Cantwell and Morton [46] emphasized that it would depend on the global structure of the impacted specimen. Choi *et al.* [44] verified that the *bending crack* in the 90° layer is caused by the combination of σ_{13}, σ_{11} and σ_{33} (Figure 2.12), for the line-loading impact damaging. Since it was verified that in comparison to σ_{13} and σ_{11}, σ_{33} is very small, it can be disregarded.

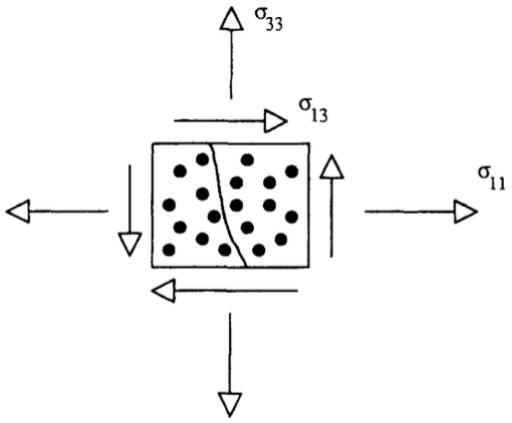

Figure 2.12: Diagram for the stress components that contribute for the bending matrix crax in the transverse layer. [20, 47]

- *Fiber failure*

The failure of the fibers mode usually occurs much later than the matrix cracking and delamination. Nonetheless and although the research around the fiber failure being small, Dorey [48] presents an equation for the fiber failure due to back surface bending.

$$Energy(E) = \frac{\sigma^2 wtl}{18E_f} \tag{2.16}$$

where, σ = flexural strength, E_f = flexural modulus, w = width, l = unsupported length and t = specimen thickness.

- *Delamination*

Delamination can be defined as a crack that runs in a resin-rich area between lamina that have a different fiber orientation but not on plies that have the same orientation of the fibers (same ply group).[20]. As explained in the work by Liu [49], is a mismatch of the bending stiffness between adjacent layers (with different fiber orientations).

Dorey [48, 50, 51] worked in this field a lot and provided a simple expression for the elastic strain energy, E, absorbed at the point of delamination failure, that suggests the delamination to occur in short span or thick laminates with low inter-laminar shear strength.

$$Energy(E) = \frac{2\tau^2 wl^3}{9E_f t} \tag{2.17}$$

where t = thickness, τ = inter-laminar shear strength, w= width,l = unsupported length and E_f =

flexural modulus.

Delamination: initiation and interaction with matrix cracking.

Impacted caused delamination only occurs after reaching a threshold energy and delamination has been observed to only occur in the presence of matrix cracking [44].

Joshi and Sun [42] concluded that when the inclined shear crack in the upper layer (Figure 2.11(a)) reaches the interface it is halted (by the change in orientation of the fibers) and so propagates between the layers as a delamination. This delamination is generally constrained by the middle transverse crack (Figure 2.11(b)) and after this crack, the process repeats itself creating delamination in the lower layers. Matrix cracks that lead to delamination are known as *critical matrix cracks* [47].

- *Penetration*

Penetration is a macroscopic phenomena where the fiber failure reaches a critical value and thus, enables the impactor to penetrate the material.

Cantwell and Morton [46] made some research on the subject of penetration present in low-velocity impacts, finding that this would change with the thickness of the impacted surface for carbon fiber reinforced plastic (CFRP). Yet again, Dorey [48] proposes a simplified equation for the calculation of the energy required for penetration.

$$Energy(E) = \pi \Gamma t D \tag{2.18}$$

where Γ = fracture energy, t = thickness of the plate and D = diameter of the impactor.

From the small review of the material behaviour, it is possible to understand that using a criteria that allows for the analysis of the modes and the interactions of each lamina with its neighbour is the best methodology. This leaves the possibility for either the Hashin or Puck model to be used and they will be presented in the subsection that follows.

2.3.1 Impact damage model

The impact damage models considered are the Puck and Hashin. These criteria both take into account the homogeneity of the material and the cross lamina stress and strength interactions.

The main difference between the criteria proposed by Puck, when compared to Hashin's, is that Puck considers the matrix to have three failure modes as can be observed on Figure 2.13.

For the work being developed, the differentiation of the matrix failure modes into three different modes presents an over-complication of the problem and this is the reason why the considered model will be the Hashin's failure criterion.

Hashin Failure Criteria

Hashin [53] proposed in 1980 a model for failure prediction on unidirectional fiber reinforced composites. This criterion contemplated, as referenced before, the inclusion of the possible failures inside the lamina: fiber and matrix failure modes.

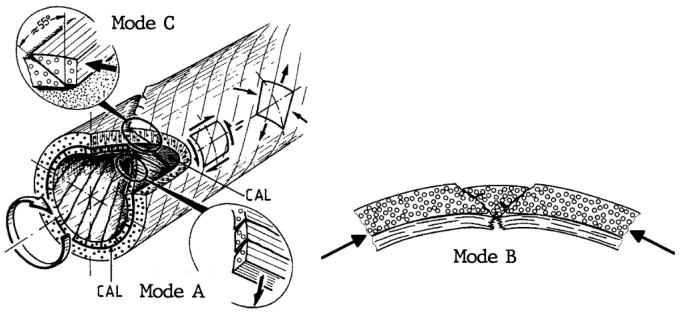

Figure 2.13: Matrix failure modes considered by Puck. [52]

But it is important, before the study of this model, to understand the behaviour of the material when subjected to impact.

Since the failure stresses are very different for the tension and compression states, the failure criteria takes into account for the failure (Fiber mode in compression or tension and matrix mode in compression or tension).

Considering that a fiber-reinforced cylindrical specimen which is referred to a system of axes x_1 in fiber direction and xx_2, x_3 in the transverse directions. It follows from the transverse isotropy that the failure criterion must be invariant under any rotation of the x_2 and x_3 axes around x_1 [53] .

As such, it is only possible to write the stresses invariants under such rotations and these are, from Mulhern *et al.* [54]:

$$I_1 = \sigma_{11}\,, \tag{2.19a}$$

$$I_2 = \sigma_{22} + \sigma_{33}\,, \tag{2.19b}$$

$$I_3 = \sigma_{23}^2 - \sigma_{22}\cdot\sigma_{33} \quad or \quad \frac{1}{4}(\sigma_{22}-\sigma_{33})^2 + \sigma_{23}^2\,. \tag{2.19c}$$

$$I_4 = \sigma_{12}^2 + \sigma_{13}^2\,. \tag{2.19d}$$

$$I_5 = 2\cdot\sigma_{12}\cdot\sigma_{23}\cdot\sigma_{13} - \sigma_{22}\cdot\sigma_{13}^2 - \sigma_{33}\cdot\sigma_{12}^2\,. \tag{2.19e}$$

Choosing a quadratic approximation, Equations 2.19 can't appear on the failure criteria and the most general transversely isotropic quadratic approximation will be:

$$A_1 I_1 + B_1 I_1^2 + A_2 I_2 + B_2 I_2^2 + C_{12} I_1 I_2 + A_3 I_3 + A_4 I_4 = 1 \tag{2.20}$$

Applying axial shear to Equations 2.19 and Equation 2.20, its possible to obtain:

$$A_3 = \frac{1}{\tau_T^2} \qquad and \qquad A_4 = \frac{1}{\tau_A^2} \tag{2.21}$$

With both Equation 2.20 and Equation 2.21 and assumptions of the fiber plane failure is on the x_2X_3 plane and that fibers under axial compression buckle in shear mode and that the matrix mode is a planar

fracture in fiber direction where there is no influence of σ_{11} but only σ_{22}, σ_{33} and σ_{23}, it is possible to find the failure criteria of both the fiber and matrix mode:

Fiber Mode

$$A_f\sigma_{11} + B_f\sigma_{11}^2 + \frac{1}{\tau_A^2}(\sigma_{12}^2 + \sigma_{13}^2) = 1 \tag{2.22}$$

Matrix mode

$$A_m(\sigma_{22} + \sigma_{33}) + B_m(\sigma_{22} + \sigma_{33})^2 + \frac{1}{\tau_T^2}(\sigma_{23}^2 - \sigma_{22}\sigma_{33}) + \frac{1}{\tau_A^2}(\sigma_{12}^2 + \sigma_{13}^2) = 1 \tag{2.23}$$

Fiber Mode

$$A_f\sigma_{11} + B_f\sigma_{11}^2 + \frac{1}{\tau_A^2}(\sigma_{12}^2 + \sigma_{13}^2) = 1 \tag{2.24}$$

- *Tensile Fiber Mode* $\sigma_{11} > 0$

With the simplification to an ellipse quadrant with axes intersected by σ_A^+ (the tensile stress in fiber directrion) and τ_A (the axial failure shear), due to the locus expected being convex, resulting the mutual weakening of the tensile σ_{11} and the shear $\sigma 12$

So, we have:

$$\left(\frac{\sigma_{11}}{\sigma_A^+}\right)^2 + \frac{1}{\tau_A^2}(\sigma_{12}^2 + \sigma_{13}^2) = 1 \tag{2.25}$$

or,

$$\sigma_{11} = \sigma_A^+ \tag{2.26}$$

- *Compressive Fiber Mode* $\sigma_{11} < 0$

Considers it to be the simple maximum stress form.

$$\sigma_{11} = -\sigma_A^- \tag{2.27}$$

Matrix Mode

$$A_m(\sigma_{22} + \sigma_{33}) + B_m(\sigma_{22} + \sigma_{33})^2 + \frac{1}{\tau_T^2}(\sigma_{23}^2 - \sigma_{22}\sigma_{33}) + \frac{1}{\tau_A^2}(\sigma_{12}^2 + \sigma_{13}^2) = 1 \tag{2.28}$$

The matrix mode is a more complex problem that after some algebraic manipulation allows to obtain two modes, one for the compressive and another for the tensile behaviours.

- *Tensile Matrix Mode* $\sigma_{22} + \sigma_{33} > 0$

$$\frac{1}{\sigma_T^{+2}}(\sigma_{22}+\sigma_{33})^2+\frac{1}{\tau_T^2}(\sigma_{23}^2-\sigma_{22}\sigma_{33})+\frac{1}{\tau_A^2}(\sigma_{12}^2+\sigma_{13}^2)=1 \tag{2.29}$$

- *Compressive Matrix Mode* $\sigma_{22}+\sigma_{33}<0$

$$\frac{1}{\sigma_T^-}\left[\left(\frac{\sigma_T^-}{2\tau_T}\right)^2-1\right](\sigma_{22}+\sigma_{33})+\frac{1}{4\tau_T^2}(\sigma_{22}+\sigma_{33})^2+\frac{1}{\tau_T^2}(\sigma_{23}^2-\sigma_{22}\sigma_{33})+\frac{1}{\tau_A^2}(\sigma_{12}^2+\sigma_{13}^2)=1 \tag{2.30}$$

Chapter 3

Implementation

3.1 Theoretical Model for the material behaviour

Composite materials can accumulate damage and, as such, it would not be correct to use only the failure criteria to predict the failure behaviour of the material and a Continuum damage model should be applied for the analysis.

From the previous Chapter 2, the constitutive equation is as follows:

$$\sigma_i = C_{ij}\epsilon_j \tag{3.1}$$

where the engineering parameters, σ_i = stresses, C_{ij} = Stiffness matrix and ϵ_j = strain. Making the orthotropic assumptions from the previous chapters, the tri-dimensional stiffness can be reduced to 9 variables obtaining the stiffness and compliance matrices in the form:

$$\Big[C_{ij}\Big] = \begin{bmatrix} C_{11} & C_{12} & C_{13} & 0 & 0 & 0 \\ & C_{22} & C_{23} & 0 & 0 & 0 \\ & & C_{33} & 0 & 0 & 0 \\ & & & C_{44} & 0 & 0 \\ & & & & C_{55} & 0 \\ Sym. & & & & & C_{66} \end{bmatrix} \tag{3.2}$$

and,

$$[S_{ij}] = [C_{ij}]^{-1} \tag{3.3}$$

where, for three directions of a material ($i, j = 1, 2, 3$), the components of the stiffness matrix are [21]:

$$C_{11} = \frac{1 - \nu_{23}\nu_{32}}{E_2 E_3 \Delta}\,, \tag{3.4a}$$

$$C_{12} = \frac{\nu_{21} + \nu_{31}\nu_{23}}{E_2 E_3 \Delta} = \frac{\nu_{12} + \nu_{32}\nu_{13}}{E_1 E_3 \Delta}\,, \tag{3.4b}$$

$$C_{13} = \frac{\nu_{21} + \nu_{31}\nu_{23}}{E_2 E_3 \Delta} = \frac{\nu_{12} + \nu_{32}\nu_{13}}{E_1 E_3 \Delta} \,. \tag{3.4c}$$

$$C_{22} = \frac{1 - \nu_{13}\nu_{31}}{E_1 E_3 \Delta} \,. \tag{3.4d}$$

$$C_{23} = \frac{\nu_{32} + \nu_{12}\nu_{31}}{E_1 E_3 \Delta} = \frac{\nu_{23} + \nu_{21}\nu_{13}}{E_1 E_3 \Delta} \,. \tag{3.4e}$$

$$C_{33} = \frac{1 - \nu_{12}\nu_{21}}{E_1 E_2 \Delta} \,. \tag{3.4f}$$

$$C_{44} = G_{12}; \qquad C_{55} = G_{23}; \qquad C_{66} = G_{13} \,. \tag{3.4g}$$

$$\Delta = \frac{1 - \nu_{12}\nu_{21} - \nu_{23}\nu_{32} - \nu_{31}\nu_{13} - 2\nu_{21}\nu_{32}\nu_{13}}{E_1 E_2 E_3} \,. \tag{3.4h}$$

Having this model as an initial formulation for a purely elastic material, it is possible to calculate the damage that occurs in the fibers and matrix and calculate new stiffness matrices that take into account the new properties after fiber or matrix damage and weakening. For this, it is necessary to calculate the strains, stiffness matrices and stresses for each iteration (noting that the first iteration considers a pure elastic state and both the strain increment and damage coefficients are set as zero).

Strains

For the calculation of the stresses and their progress during the analysis, a strain increment is included in the strain matrix which updates the strain for each iteration of the failure analysis. As such:

$$\epsilon_{new} = \epsilon_{old} + \epsilon_{increment} \tag{3.5}$$

Where, ϵ_{new} is the strain for the current iteration, ϵ_{old} is the strain for the previous iteration and the $\epsilon_{increment}$ is the strain increment given for the calculations of the current iteration.

Damaged Stiffness Matrix

Using the Linde *et al.* [55] formulation for the damaged stiffness matrix expanded for the three dimensional model, is possible to have the degraded stiffness matrix as follows:

.

$$\left[C_{ij}^{d}\right] = \begin{bmatrix} (1-d_f)C_{11} & (1-d_f)(1-d_m)C_{12} & (1-d_f)C_{13} & 0 & 0 & 0 \\ & (1-d_m)C_{22} & (1-d_m)C_{23} & 0 & 0 & 0 \\ & & C_{33} & 0 & 0 & 0 \\ & & & (1-d_f)(1-d_m)G_{12} & 0 & 0 \\ & & & & (1-d_m)G_{23} & 0 \\ Sym. & & & & & (1-d_f)G_{13} \end{bmatrix} \tag{3.6}$$

where, d_f is the fiber damage, d_m is the matrix damage and are defined by:

$$d_f = 1 - (1 - d_{ft})(1 - d_{fc})\,, \tag{3.7a}$$

$$d_m = 1 - (1 - S_{mc}d_{mt})(1 - S_{mc}d_{mc})\,, \tag{3.7b}$$

Where d_f is the fiber damage component in function of the tensile and compressive fiber damage (d_{ft} and d_{fc} respectively). The matrix damage (d_m) is given in function of the tensile and compressive matrix damage (d_{ft} and d_{fc} respectively) and the coefficients S_{mt} and S_{mc} are to control the shear stiffness due to matrix damage and can be set as $S_{mt} = 0.9$ and $S_{mc} = 0.5$ (from [56], [57], [58]) or can be set as $S_{mt} = S_{mc} = 0.93$ from[59]. Since Zhou *et al.* made a study regarding the best parameter to use and the results were that the best was to set these parameter to a range between 0.93 and 0.96, this model will consider the parameter to be 0.93. However it would be important to study the influence of this parameter on the results in future works.

It's important to note that for the stiffness matrix Wang *et al.* [60] used the principle energy to propose a possible degradation stiffness matrix and it is as follows:

.

$$\left[C_{ij}^{d}\right] = \begin{bmatrix} (1-d_1)^2C_{11} & (1-d_1)(1-d_2)C_{12} & (1-d_1)(1-d_3)C_{13} & 0 & 0 & 0 \\ & (1-d_2)^2C_{22} & (1-d_m)C_{23} & 0 & 0 & 0 \\ & & (1-d_3)^2C_{33} & 0 & 0 & 0 \\ & & & (1-d_4)^2G_{12} & 0 & 0 \\ & & & & (1-d_5)^2G_{23} & 0 \\ Sym. & & & & & (1-d_6)^2G_{13} \end{bmatrix} \tag{3.8}$$

where,

$$d_1 = d_f = 1 - (1 - d_{ft})(1 - d_{fc})\,, \tag{3.9a}$$

$$d_2 = d_m = 1 - (1 - S_{mc}d_{mt})(1 - S_{mc}d_{mc})\,, \tag{3.9b}$$

$$d_3 = 0\,. \tag{3.9c}$$

$$d_4 = d_5 = d_6 = 1 - (1 - d_f)(1 - d_m)\,. \tag{3.9d}$$

This type of degraded stiffness matrix was found to produce better results for low velocity impacts of higher energy values than the ones that will be considered in this study and, as such the matrix considered will be the one from Linde *et al.* (Equation 3.6).

Stresses

With the calculation of the strains and the damaged stiffness matrix, it is possible to calculate the new stress state for each iteration:

$$\sigma_i = C_{ij}^d \epsilon_j \tag{3.10}$$

Failure Evaluation

Hashin Failure Criteria

As previously mentioned, the failure criteria to use for this case will be the Hashin failure criteria that, for reading simplicity, will be re-writen here:

Fibre Mode

- *Tensile Fibre Mode* $\sigma_{11} > 0$

$$\left(\frac{\sigma_{11}}{\sigma_A^+}\right)^2 + \frac{1}{\tau_A^2}(\sigma_{12}^2 + \sigma_{13}^2) = 1 \tag{3.11}$$

or,

$$\sigma_{11} = \sigma_A^+ \tag{3.12}$$

- *Compressive Fibre Mode* $\sigma_{11} < 0$

$$\sigma_{11} = -\sigma_A^- \tag{3.13}$$

Matrix Mode

- *Tensile Matrix Mode* $\sigma_{22} + \sigma_{33} > 0$

$$\frac{1}{\sigma_T^{+2}}(\sigma_{22} + \sigma_{33})^2 + \frac{1}{\tau_T^2}(\sigma_{23}^2 - \sigma_{22}\sigma_{33}) + \frac{1}{\tau_A^2}(\sigma_{12}^2 + \sigma_{13}^2) = 1 \tag{3.14}$$

- *Compressive Matrix Mode* $\sigma_{22} + \sigma_{33} < 0$

$$\frac{1}{\sigma_T^-}\left[\left(\frac{\sigma_T^-}{2\tau_T}\right)^2 - 1\right](\sigma_{22} + \sigma_{33}) + \frac{1}{4\tau_T^2}(\sigma_{22} + \sigma_{33})^2 + \frac{1}{\tau_T^2}(\sigma_{23}^2 - \sigma_{22}\sigma_{33}) + \frac{1}{\tau_A^2}(\sigma_{12}^2 + \sigma_{13}^2) = 1 \tag{3.15}$$

Yarn introduction

As previously stated, Shah *et al.* [28] presented two possible solutions for the modelling of tensile failure on natural fiber reinforced composites: One was with the assumption that the yarns could be considered as a flat surface and, with the application of the off-axis case of the Tsai-Hill criteria. The other was a fitting of a $cos(2\alpha)$ curve to the experimental data. Since the data for impact is rather limited for this types of composites and a generalised model for the prediction of the behaviour in this conditions is preferred, the path that was used was that of the simplification of the yarn into a plate with off-axis loading where the loading angle corresponds to the fiber angle (see Figure 2.8).

As such, considering a simplification of the Hashin failure criteria to an in-plane analysis due to the thickness of each plate being much smaller than the other two dimensions, we have:

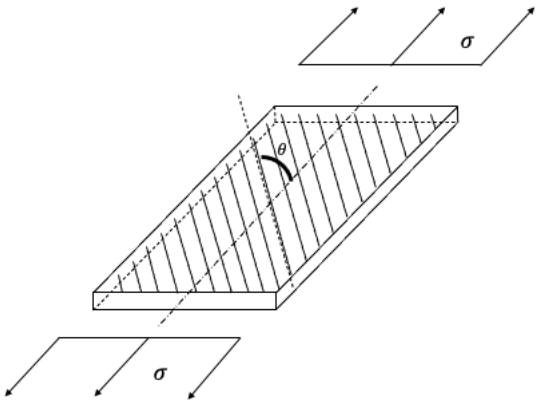

Figure 3.1: Off-axis specimen with applied tension.

- Tensile Fiber Mode

$$\left(\frac{\sigma_{11}}{\sigma_A^+}\right)^2 + \left(\frac{\sigma_{12}}{\tau_A}\right)^2 = 1, \qquad \sigma_{11} > 0 \tag{3.16}$$

- Compressive Fiber Mode

$$\sigma_{11} = -\sigma_A^- \qquad \sigma_{11} < 0 \tag{3.17}$$

- Tensile Matrix Mode

$$\left(\frac{\sigma_{22}}{\sigma_T^+}\right)^2 + \left(\frac{\sigma_{12}}{\tau_A}\right)^2 = 1, \qquad \sigma_1 1 > 0 \tag{3.18}$$

- Compressive Matrix Mode

$$\left(\frac{\sigma_{22}}{2 \cdot \tau_T}\right)^2 + \left[\left(\frac{\sigma_T^-}{2\tau_T}\right)^2 - 1\right] \cdot \left(\frac{\sigma_{22}}{\sigma_T^-}\right) + \left(\frac{\sigma_{12}}{\tau_A}\right)^2 = 1 \tag{3.19}$$

Considering a tension applied unidirectionally as it's possible to view in Figure 3.1, and following Hashin's [53] formulations, we can obtain:

$$\sigma_{11} = \sigma \cdot cos^2(\theta)\,, \tag{3.20a}$$

$$\sigma_{22} = \sigma \cdot sin^2(\theta)\,, \tag{3.20b}$$

$$\sigma_{12} = \sigma \cdot sin(\theta) \cdot cos(\theta) \tag{3.20c}$$

and, introducing them in Equations 3.16 and 3.18, it's possible to obtain the off-axis failure stresses as follows:

$$\sigma_{fu} = \frac{1}{cos^2(\theta)\left[\frac{cos^2(\theta)}{\sigma_T^2} + \frac{sin^2(\theta)}{\tau_A^2}\right]} \tag{3.21}$$

for the fiber ultimate stress,

$$\sigma_{mu} = \frac{1}{sin^2(\theta)\left[\frac{sin^2(\theta)}{\sigma_T^2} + \frac{cos^2(\theta)}{\tau_A^2}\right]} \tag{3.22}$$

for the matrix ultimate stress.

For the value of θ, the findings of Madsen *et al.* [36] where a correlation between the average off-axis angle (θ) and the fiber surface twist angle, we have:

$$\theta_{mean} = \alpha + \frac{\alpha}{tan^2(\alpha)} - \frac{1}{tan(\alpha)} \tag{3.23}$$

As for the value of α (the surface twist angle) it can be obtained by using the staple yarn definition of Hearle *et al.* [29] (where the yarn cross-section is assumed to be circular) by the following equation:

$$tan(\alpha) = \frac{2\pi r}{L} = 2\pi r T \tag{3.24}$$

where, L is the lenght of the yarn for one turn, r is the fiber radius and T is the twist level (also defined as $1/L$).

Pan [37] on his work states that the surface twist angle of the yarn is better given by 2α due to the double helix configuration that the twisted yarn presents.

With this, we have the proposed model for the impact behaviour of a composite material reinforced by unidirectional flax fibers (yarns) as follows:

Fibre Mode

- *Tensile Fibre Mode* $\sigma_{11} > 0$

$$\left(\frac{\sigma_{11}}{\sigma_{fu}}\right)^2 + \frac{1}{\tau_A^2}(\sigma_{12}^2 + \sigma_{13}^2) = 1 \tag{3.25}$$

or,

$$\sigma_{11} = \sigma_{fu} \tag{3.26}$$

- *Compressive Fibre Mode* $\sigma_{11} < 0$

$$\sigma_{11} = -\sigma_A^- \tag{3.27}$$

Matrix Mode

- *Tensile Matrix Mode* $\sigma_{22} + \sigma_{33} > 0$

$$\frac{1}{\sigma_{mu}}(\sigma_{22} + \sigma 33)^2 + \frac{1}{\tau_T^2}(\sigma_{23}^2 - \sigma_{22}\sigma_{33}) + \frac{1}{\tau_A^2}(\sigma_{12}^2 + \sigma_{13}^2) = 1 \tag{3.28}$$

- *Compressive Mode* $\sigma_{22} + \sigma_{33} < 0$

$$\frac{1}{\sigma_T^-}\left[\left(\frac{\sigma_T^-}{2\tau_T}\right)^2 - 1\right](\sigma_{22}+\sigma_{33}) + \frac{1}{4\tau_T^2}(\sigma_{22}+\sigma_{33})^2 + \frac{1}{\tau_T^2}(\sigma_{23}^2 - \sigma_{22}\sigma_{33}) + \frac{1}{\tau_A^2}(\sigma_{12}^2+\sigma_{13}^2) = 1 \qquad (3.29)$$

Studies regarding the impact of the twist angle of the fibers constituting a yarn on the mechanical behaviour under compressive load are scarce and/or non-existent and, as such, the Hashin failure criteria model for the Compressive Fiber Mode will remain in the original formulation.

3.2 Numerical Model

In order to simulate the low velocity impact in a flax yarn reinforced laminated composite plate, the numeric solver Abaqus/Explicit was used for the modelling and processing of the test simulation. A user subroutine VUMAT was developed in order to allow for the introduction of the material specific characteristics as well as the modification of the criteria defining the material behaviour in order to allow for the modifications mentioned in the previous section.

The subroutine is written using the programming language Fortran and is able to link with Abaqus. It had a default interface defined in the Abaqus/Explicit documentation [61] and shown in Figure 3.2.

```
      subroutine vumat(
C Read only (unmodifiable)variables -
     1  nblock, ndir, nshr, nstatev, nfieldv, nprops, lanneal,
     2  stepTime, totalTime, dt, cmname, coordMp, charLength,
     3  props, density, strainInc, relSpinInc,
     4  tempOld, stretchOld, defgradOld, fieldOld,
     5  stressOld, stateOld, enerInternOld, enerInelasOld,
     6  tempNew, stretchNew, defgradNew, fieldNew,
C Write only (modifiable) variables -
     7  stressNew, stateNew, enerInternNew, enerInelasNew )
C
      include 'vaba_param.inc'
C
      dimension props(nprops), density(nblock), coordMp(nblock,*),
     1  charLength(nblock), strainInc(nblock,ndir+nshr),
     2  relSpinInc(nblock,nshr), tempOld(nblock),
     3  stretchOld(nblock,ndir+nshr),
     4  defgradOld(nblock,ndir+nshr+nshr),
     5  fieldOld(nblock,nfieldv), stressOld(nblock,ndir+nshr),
     6  stateOld(nblock,nstatev), enerInternOld(nblock),
     7  enerInelasOld(nblock), tempNew(nblock),
     8  stretchNew(nblock,ndir+nshr),
     8  defgradNew(nblock,ndir+nshr+nshr),
     9  fieldNew(nblock,nfieldv),
     1  stressNew(nblock,ndir+nshr), stateNew(nblock,nstatev),
     2  enerInternNew(nblock), enerInelasNew(nblock)
C
      character*80 cmname
C

      do 100 km = 1,nblock
        user coding
  100 continue
```

Figure 3.2: Interface for the VUMAT user subroutine [61].

The subroutine, with the basic description shown in Figure 3.3, has the material properties introduced via a $1 \times n$ matrix and are set in the model created in the Abaqus/Explicit CAE environment. This input matrix includes, for the present implementation, the three dimensional material properties for the Elasticity (E) and Shear (G) Moduli, Poisson ratios (ν_{ij}), Ultimate Normal (σ) and Shear (τ) Stresses

and Density (ρ). It is also passed on information about the simulation that can be observed on Figure 3.2. The variables observed on Figure 3.2 will be enunciated on Appendix B

With the material and simulation parameters inserted, the subroutine starts by assuming a purely elastic material and calculates a non-deformed stiffness matrix (C_{ij}) using the Equations 3.4. With the stiffness matrix and the initial values of the stresses and strains, as well as the ultimate stresses and strains, it proceeds to do a failure evaluation using the Hashin failure criteria (either modified or non-modified, depending on the analysis) and evaluates the damage and if failure is achieved.

With every iteration, a strain increment is imputed from the Abaqus/Explicit model and added to the initial strain. From this, a deformed stiffness matrix is calculated using the model in Equation 3.6 and the stresses are updated initiating a new failure evaluation.

As an output, the VUMAT allows for the update of the "SDV" parameters that, in the present study, where set as the outputs for the failure of the various modes of the Hashin failure criteria. It allows also for the update in the Abaqus/Explicit model of the new stresses, strains and internal energies.

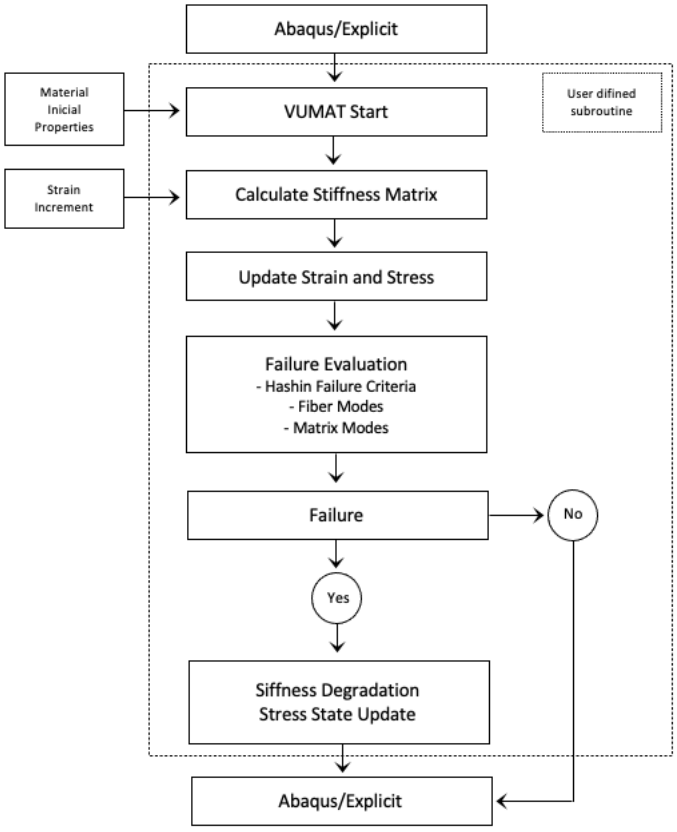

Figure 3.3: VUMAT user subroutine flow chart for the procedure for the project analysis.

3.3 Verification and Validation

For the validation of the proposed model, the experimental procedures and results from Sy *et al.* [62] were considered.

The experiments consisted on an emulation of the drop weight impact test on a unidirectional flax/e-

poxy laminate. The flax fiber material used in the manufacturing of the composite laminate was a quasi-unidirectional flax fiber fabric, FlaxPly® UD-150 which properties are listed on Table 3.1 [63]

Property	Value	Unit
Density	$1,45$	g/cm^3
Areal Weight	1.52	g/cm^2
Areal Volume	0.106	mm^3/mm^2
Thickness	0.165	mm
Weave style	ribs 4/4	–
Yarns/cm	52	$warp$
Picks/cm	3	$weft$
Turns/cm	5	$turns/cm$

Table 3.1: FlaxPly® UD-150 properties [63]

It's important to note that Sy *et al.* found that the diameter of the yarns would vary between $150\mu m$ and $250\mu m$. Another important observation is that the fabric has yarns in the perpendicular direction to the main one, the approximation can be made to an unidirectional material due to the much lower quantity of these perpendicular yarns.

The numerical simulations will consider five impact scenarios with the energies being $5J$, $7J$, $8J$, 9 and $10J$.

The validation of the results for the model developed will be made by comparing the dissipated energy of the simulations on Abaqus/Explicit and the experimental results measured by Sy *et al.*.

The dissipated energy will be measured via the kinetic energy after the re-bounce of the impactor:

$$E_{absorbed} = E_{Inicial} - E_{kinetic_{final}} \tag{3.30}$$

This values will be compared with the experimental values on Table 3.2:

Impact Energy (J)	Absorbed Energy (J)
5	2.89
7	4.64
8	5.14
9	6.07
10	10

Table 3.2: Experimental results from Sy *et al* for the energy absorved on impact [62]

From the comparison of the results, the conclusions will be drawn.

Chapter 4

Numerical Analysis

For the simulation of the proposed model, as was mentioned in Chapter 3, the Abaqus/Explicit solver will be used. For this Finite Element Analysis, a model of the experimental test from Sy *et al.* [62] was created.

4.1 Modelling

In order to simulate a drop weight experimental procedure, the model created consists on the creation of two parts, being them the impactor and the composite plate.

4.1.1 Simulation model

Impactor

For the impactor, a three dimensional discrete rigid part was created, making the assumption that using this type of non-deformable part would allow the disregard of the attribution of a material that would be much stronger than the composite plate.

The impactor presents a semi-spherical and a cylindrical sections, being the semi-spherical section the one which dimensions matter the most, since it is the section that directly contacts with the composite plate. The diameter for this section is of $16mm$.

For the attribution of mass to the part, a reference point was created on the central axis of the part and in the Abaqus/Explicit CAE properties module, making use of the menu "Special > Inertia > Create", a mass of $4.4kg$ was set on the Reference Point previously created and, with this, the impactor was modelled.

Composite Plate

For the modelling of the composite plate, the assumption was made that it would be set as a plate of thickness $3.7mm$. With this in mind, a part of the type "Deformable" was generated with a solid extrusion. The final dimensions of the plate, as per Sy *et all* [62] were $127mm \times 127mm \times 3.7mm$.

In order to mimic the behaviour of a laminated composite, 16 sections of equal thickness ($0.23125mm$) were created using the creation of datum planes and the option "Partition Cell: Use Datum Plane" on the "Part" menu.

It was also created a partition section of the faces on the impact plane using the features "Partition Face: Sketch" and "Partition Cell: Extrude/Sweep Edges" in order to create an impact zone that would allow for a finer refinement of the mesh without a considerable increase of the simulation time, as well as the contact zone for the contact between impactor and composite to be set.

Assembly

The assembly of both parts described in the previous section is shown here.

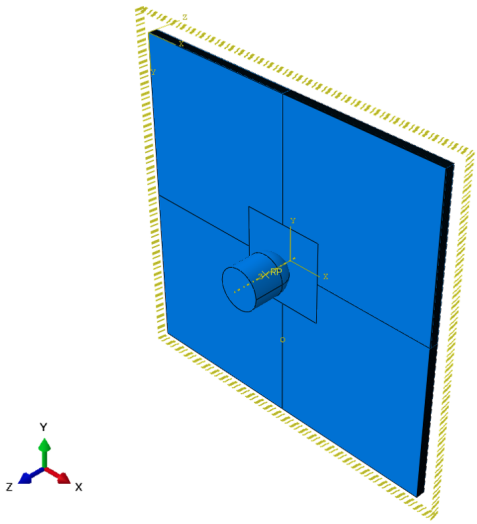

Figure 4.1: Assembly of the described impactor and composite plate.

It's important to note that the impactor and composite parts are not touching but have a very small seperation ($0.1mm$) in order to simulate the instant before impact.

4.1.2 Properties

For the properties assignment, the data from Mahboob *et al.* [64] was used and is shown on Table 4.1 for the tension and compression cases.

Making use of the properties module on Abaqus/Explicit CAE, it is possible to create a material to be assigned to the composite material. Since the objective is to make use of a VUMAT subroutine, when creating the material there are some steps that we have to follow. First, on the creating the material window, we can assign the density directly on Abaqus/Explicit with "General > Density", then it was generated a Depvar, using also "General > Depvar" which is needed to set the number of solution-dependent state variables to be calculated on the VUMAT subroutine (it was set at 17 in the present case) and the VUMAT variable number responsible for controlling element deletion (this case set as 5). With this, the last step is to introduce the User material ("General > User Material") with the properties needed to be considered on an array that will be passed on to the VUMAT subroutine. Since

	Tension			Compression		
Property Group	Property	Value	Unit	Property	Value	Unit
Modulus	E_{11}^t	31.42 ± 1.47	GPa	E_{11}^c	30.32 ± 3.04	GPa
	E_{22}^t	5.58 ± 0.5	GPa	E_{22}^c	5.70 ± 0.71	GPa
	G_{12}^t	2.07 ± 0.13	GPa	G_{12}^c	1.63 ± 0.25	GPa
Poisson's Ratio	ν_{12}^t	0.353 ± 0.011	–	ν_{12}^c	0.396 ± 0.046	–
	ν_{21}^t	0.067 ± 0.003	–	ν_{21}^c	0.066 ± 0.010	–
Ultimate Strength	σ_{11}^{tu}	286.70 ± 13.30	MPa	σ_{11}^{cu}	127.11 ± 5.08	MPa
	σ_{22}^{tu}	33.86 ± 1.35	MPa	σ_{22}^{cu}	79.94 ± 9.95	MPa
	τ_{11}^{tu}	37.35 ± 1.78	MPa	τ_{11}^{cu}	43.24 ± 0.52	MPa
Ultimate Fail Strain	ϵ_{11}^{tu}	1.53 ± 0.07	%	ϵ_{11}^{cu}	1.60 ± 0.29	%
	ϵ_{22}^{tu}	1.36 ± 0.18	%	ϵ_{22}^{cu}	2.61 ± 0.53	%
	γ_{12}^{tu}	14.92 ± 2.57	%	γ_{12}^{cu}	9.76 ± 2.63	%
Density	ρ	1310	kg/m^3	ρ	1310	kg/m^3

Table 4.1: Mechanical properties of an unidirectional 16 layer Flax/Epoxy Composite under tension and compression [64].

the material being considered is assumed to be three-dimensional, some assumptions were made for using the properties on Table 4.1, and are described as follows:

Property	Value	Units
E_{11}	31.42	GPa
E_{22}	5.58	GPa
E_{33}	5.58	GPa
ν_{12}	0.353	–
ν_{13}	0.353	–
ν_{23}	0.403	–
G_{12}	2.07	GPa
G_{13}	2.07	GPa
G_{23}	1.035	GPa
σ_1^{tu}	286.70	MPa
σ_1^{cu}	127.11	MPa
σ_2^{tu}	33.86	MPa
σ_2^{cu}	79.94	MPa
σ_3^{tu}	33.86	MPa
σ_3^{cu}	79.94	MPa
τ_{12}^u	37.35	MPa
τ_{13}^u	37.35	MPa
τ_{23}^u	37.35	MPa
ρ	1310	kg/m^3
β_{damp}	$1.9E^{-8}$ [65]	–
$cos^2(\theta)$	0.0689	–
$sin^2(\theta)$	0.93106	–

Table 4.2: Properties used on the definition of the user material.

Where the properties $cos^2(\theta)$ and $\sin^2(\theta)$ were obtained from Equations 3.23 3.24 re-written here:

$$tan(\alpha) = \frac{2\pi r}{L} = 2\pi r T \Leftrightarrow \alpha = tan^{-1}\left(\frac{2\pi r}{L}\right) \tag{4.1}$$

where, from the measurements of Sy *et al.* [62] the diameter was assumed to be the mean value of $150\mu m$ and $250\mu m$, (i. e. $200\mu m$) and, as such the radius was to be $100\mu m$ or $0.1mm$. L is the length of one turn wich from Table 3.1 is known to be 5 turns per cm and it means that $L = 2mm$

with this,

$$\alpha = tan^{-1}\left(\frac{2\pi r}{L}\right) = 17.44^{o} \tag{4.2}$$

Again, using Pan [37] model of the yarn being better represented by 2α due to the double helix configuration,

$$\alpha = 34.88^{o} \tag{4.3}$$

with this, is possible to calculate θ:

$$\theta_{mean} = \alpha + \frac{\alpha}{tan^2(\alpha)} - \frac{1}{tan(\alpha)} = 105,22^{o} \tag{4.4}$$

To finish, it is possible to define one more property to the contact between the impactor and the composite plate using the module "Interaction" to create an interaction between the two parts defined on the elements that constitute the impact region and assign a tangential behaviour with a penalty of 0.3 and a normal behaviour as "Hard Contact".

Step definition

For the analysis to occur, a step were the numerical procedure for the model is created. With this in mind, using the Abaqus/Explicit module "*Step*", a step was created with the procedure type "Dynamic, Explicit".

On this type of procedure, the user can define the parameters and the analysis time for the simulation. In order to set this time value numerical simulations were made and it was set as 20 to 25 milliseconds for the whole analysis (i. e. beginning, impact and rebound) depending on the impact energy. The "Incrementation", "Mass scaling" and "Other" tabs were all left at default values.

In this module is also possible to ask for the outputs to be used on the post processing analysis. The outputs can be in two natures: Field output and History output.

Field output

This type of output allowed for the assignment of the increment number for the analysis and was set as 100.

From this type of output, it was asked eleven different outputs for the whole model:

- Stress components and invariants (S);
- Volume-averaged stress components and invariants (SVAVG);
- Plastic Strain Components (PE);
- Volume-averaged plastic strain components (PEVAVG);
- Equivalent plastic strain (PEEQ);
- Logarithmic strain components (LE);
- Translations and rotations (U);

- Translational and rotational velocities (V);
- Translational and rotational accelerations (A);
- Solution dependent state variables (SDV) - from the VUMAT;
- Status (STATUS) - from the VUMAT.

History outputs

For this type of outputs, two groups were created. One is applied to the whole model where the energies verified through the simulation were shown (Kinetic energy and total energy). The other was applied to the impactor in order to measure it's velocity and displacement throughout the simulation. For this analysis, the quantity of increments was set as 200 on both the created History outputs.

4.1.3 Loads and boundary conditions

Boundary conditions

For the simulation of the experiment, in the Finite Element Model, two boundary conditions had to be applied to simulate a drop weight impact.

One of the conditions was applied to the composite and it was applied on the Abaqus/Eplicit using the module "Load" and with the "Boundary Condition Manager", a boundary condition of the type "Symmetry/Antisymmetry/Encastre" where an "Encastre" was defined to all the sides of the composite (edges of each section) restricting it's movement either by translation ($U_1 = U_2 = U_3 = 0$) or by rotation ($UR_1 = UR_2 = UR_3 = 0$).

The other boundary condition was applied to the impactor part and it was defined in the same manner as the previous one but it was from the type "Displacement/Rotation" where all the displacement degrees of freedom were constrained except the translational movement on the "z-axis" ($U_1 = U_2 = UR_1 = UR_2 = UR_3 = 0$). This was in order to only allow the impactor moving on the vertical direction to the plate simulating the drop weight test.

Loads

The only load working on this simulation would be derived from the pre-defined impact energy. As such, a "Predefined field" was generated for the attribution of velocity to the impactor.

Impact Energy (J)	Impact Velocity (m/s)
5	1.50756
7	1.78377
8	1.90693
9	2.0226
10	2.13201

Table 4.3: Impact energies and correspondent impact velocities.

These velocities were calculated using the impact energy that was defined using the formula for the calculation of the kinetic energy:

$$E_{kinetic} = \frac{1}{2}mv^2 \Leftrightarrow v = \sqrt{\frac{2E_{kinetic}}{m}} \tag{4.5}$$

where, $E_{kinetic}$ is the kinetic energy of the impactor in the different tests, m is the mass of the impactor ($m = 4.4kg$) and v is the impact velocity. The different test energies as well as the impact velocities are available on Table 4.3.

4.1.4 Meshing

An important part of the Finite Element Analysis is the meshing of the parts that will actively influence the simulation. In this case there were two parts interacting and both had to have a mesh applied to them.

The type of elements chosen and it's characteristics are described on Table 4.4

Element Assignement	
Element library	Explicit
Family	3D Stress
Geometric Order	Linear
Element Type	Hex $C3D8R$

Table 4.4: Mesh element properties chosen for the simulation.

The element type is, as seen in the table, the $C3D8R$, is an 8-node element with reduced integration and hourglass control.

The accuracy of the Finite Element Analysis is directly connected to the mesh refinement or to the quantity of elements of the mesh. Since the greater the number of mesh elements, the greater computational cost, a study was made in order to find the result convergence for the absorbed energy with incremental adjustments to the mesh element size/quantity. Furthermore, and as was mentioned before, an impact zone was defined in order to allow for a better analysis of the impact zone without a greater computational cost (it allows for a better refinement of the impact zone without refining the whole plate).

The impactor mesh was set with elements of size $0.001m$ since visually it was the size that would distort less the form of the impactor. The plate mesh refinement analysis will be available on the Chapter 5 with the rest of the results obtained for the simulations. Figure 4.2 shows an example of a mesh used for the Finite Element Analysis.

4.1.5 Simulation Job

For the Finite Element Analysis, the Abaqus/Explicit module was used to create a "Job".

The "Job" created was a "Full analysis" and the option for the use of a user subroutine was used and the VUMAT subroutine was linked to the analysis with this. The option of "Parallelization" was used to allow for a faster analysis and the number of processors depended on CPU availability, with the

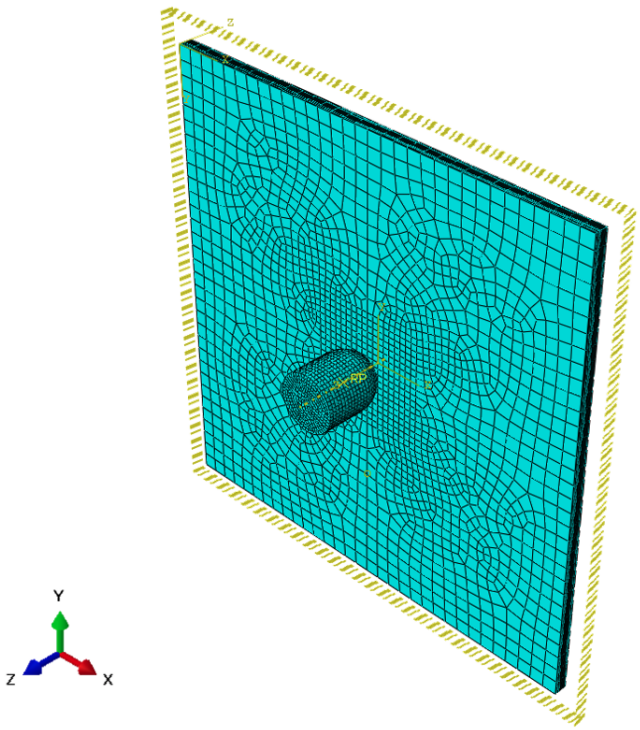

Figure 4.2: Example of a mesh applied to the assembly for simulation purposes.

multiprocessing mode set as "Threads". The machine used for the simulations was the shared ICALC7 from *Departamento de Engenharia Mecânica* of *Instituto Superior Técnico* with a 24 logic processors and 128*Gb* of RAM. For the simulation, 20 logic processors and 2Gb of Ram were used and the simulation time was between 1 and 2 hours.

At last, the analysis precision for the Abaqus/Explicit required was "Double - analysis + packager" and the Nodal output was set as "Full".

Chapter 5

Results

In this chapter, the results from the Finite Elements Analysis for the low velocity impact on a square plate, with the developed model and implementation via VUMAT on Abaqus/Explicit, are presented for various impact energy values as well as a comparison between the model presented and the experimental results obtained by Sy *et al.*.

5.1 Finite Element Analysis

5.1.1 Convergence study

As mentioned in the previous chapter, in order to obtain more accurate results, a finer mesh is ideally used. Since the number of elements used is directly related to the computational time, a convergence study for the simulation results was made, refining the impact zone until the variation between results was not very significant. This study is presented on Figure 5.1 and it's detailed on Table 5.1.

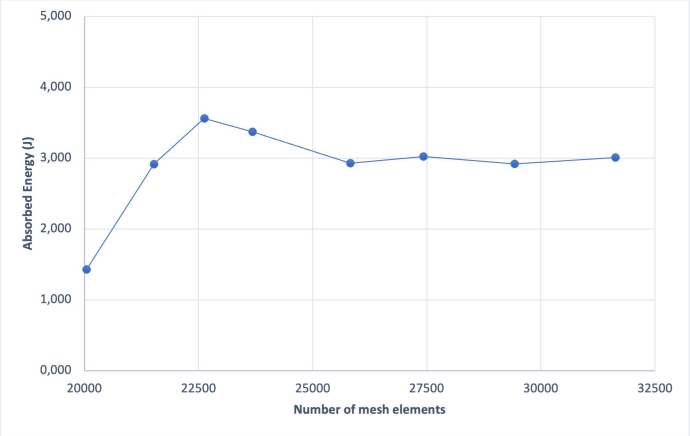

Figure 5.1: Mesh refinement study for the impact test on a plate for the impact energy of 5J.

The convergence study was finished without achieving a perfect convergence since the difference between the four last iterations was not very significant and the slight variations in the results could be a consequence of numeric errors introduced by the mesh not being uniform.

Outer Plate Element Size (mm)	Impact Zone Element Size (mm)	Number of Elements	Inicial Kinetic Energy (J)	Final Kinetic Energy (J)	Absorbed Energy (J)
$0,004$	$0,004$	20050	5	$3,571$	$1,429$
$0,004$	$0,0035$	21522	5	$2,084$	$2,916$
$0,004$	$0,003$	22626	5	$1,442$	$3,558$
$0,004$	$0,00275$	23682	5	$1,627$	$3,373$
$0,004$	$0,0025$	25826	5	$2,074$	$2,926$
$0,004$	$0,00225$	27426	5	$1,978$	$3,022$
$0,004$	$0,002$	29426	5	$2,080$	$2,920$
$0,004$	$0,00175$	31634	5	$1,993$	$3,007$

Table 5.1: Mesh convergency study for an impact velocity of $5J$.

5.1.2 Results for the various impact energies

The results of the impact analysis for the various analysis made are now presented.

Kinetic Energy

As stated on Chapter 3, the validation of the results obtained using the presented model will be done through the comparison between the absorbed energies measured on the experimental procedure and the ones calculated on the numerical analysis. As such, during the numerical analysis, the kinetic energy for the model was calculated.

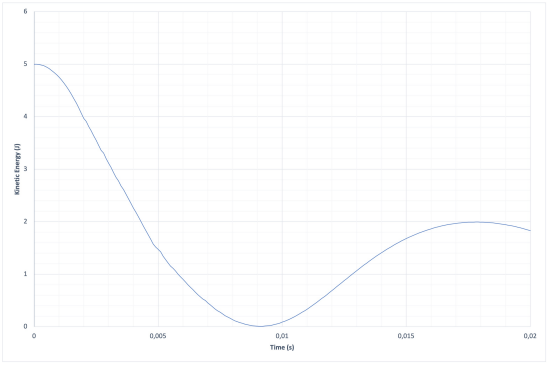

Figure 5.2: Kinetic energy variation during impact test time for initial energy of 5J.

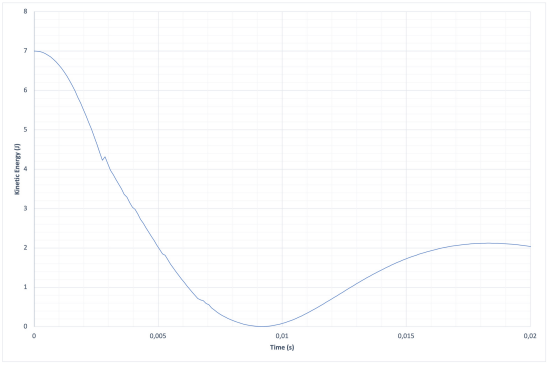

Figure 5.3: Kinetic energy variation during impact test time for initial energy of 7J.

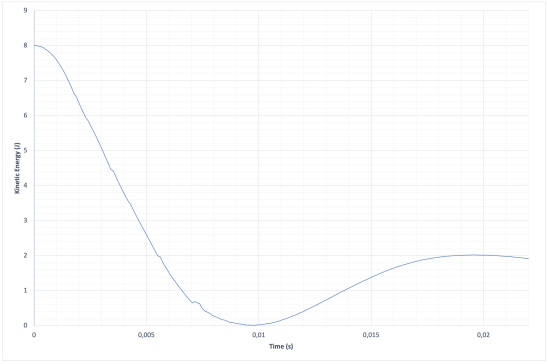

Figure 5.4: Kinetic energy variation during impact test time for initial energy of 8J.

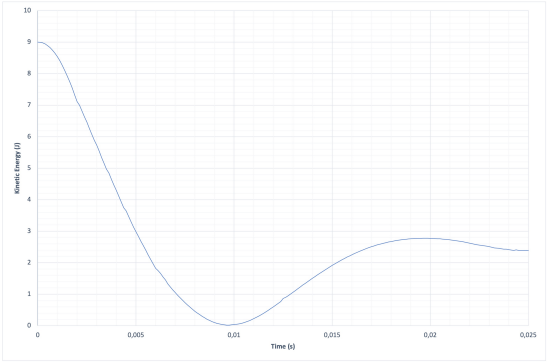

Figure 5.5: Kinetic energy variation during impact test time for initial energy of 9J.

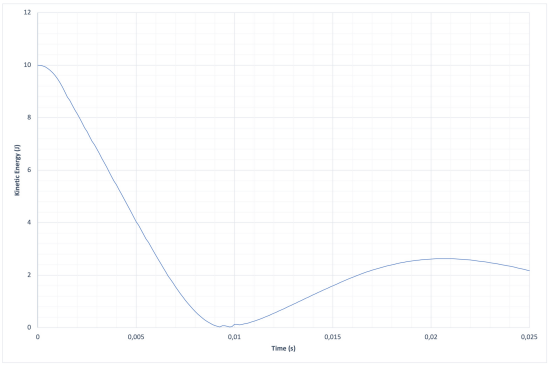

Figure 5.6: Kinetic energy variation during impact test time for initial energy of 10J.

The absorbed energy was calculated as the difference between the initial energy for each impact test and the maximum kinetic energy measured for the impactor rebound movement.

$$E_{absorbed} = E_{Inicial} - E_{kinetic_{final}} \tag{5.1}$$

It is possible to visualise, on Figures 5.2, 5.3, 5.4, 5.5 and 5.6 the variation of the kinetic energy during the numeric analysis step time. The maximum energy measured for the impactor rebound on each of the cases is shown on Table 5.2.

It is noteworthy that all the numeric analysis of the impact are creating a progressive decrease on the kinetic energy distribution and, when reaches a minimum, this decrease is followed by a continuous increase. This is not verified on the simulation of the impact with the energy of $10J$. This might be due to, in the experimental investigation, this energy being totally absorbed since there is a complete failure of the plate under analysis which does not happen in the simulation of this specific case.

Inicial Kinetic Energy (J)	Final Kinetic Energy (J)	Absorbed Energy (J)
5	$1,993$	$3,007$
7	$2,289$	$4,711$
8	$2,757$	$5,243$
9	$2,775$	$6,225$
10	$2,633$	$7,367$

Table 5.2: Inicial, maximum from rebound and absorbed energies for the various cases.

Plate Deformation

Abaqus/Explicit also allowed for the visualization of the stress evolution, damage and distortion through the plate during the impact analysis. Figures 5.7, 5.8, 5.9, 5.10, 5.11 and 5.12 show three frames of the analysis in order to represent the composite plate deformation and stress evolution in three points of the simulation. Figures 5.7 and 5.8 show a frame at the beginning of the simulation. Figures 5.9 and 5.10 are snapshots of the point of lowest (absolute) velocity where the penetration of the impactor came to a halt and after which the rebound was initiated. Figures 5.11 and 5.12 show the final state of the plate, at the end of the analysis where the rebound stopped. In all the figures mentioned, it is

possible to observe the (expected) appearance of a crack on the perpendicular direction to that of the fibers direction.

It is possible to observe the elements distortion and in Figures 5.15 and 5.16 the example for the fiber compressive failure is illustrated showing elements that had met the failure criteria. The deletion of some of these elements might explain the lack of stress concentrations on the edge of the back of the plate in the example from Figure 5.10.

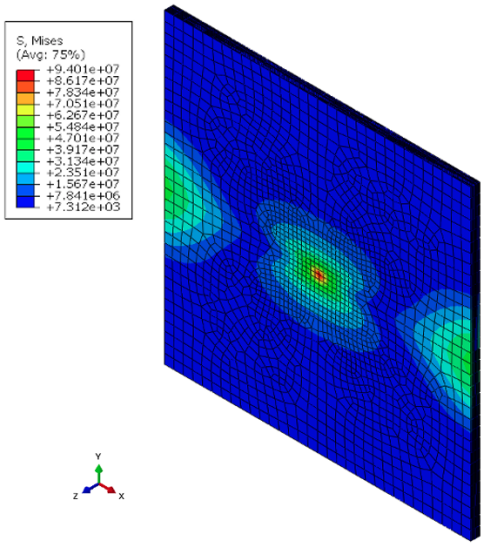

Figure 5.7: Stress distribution at the beginning of the analysis for initial impact energy of $8J$ (front view).

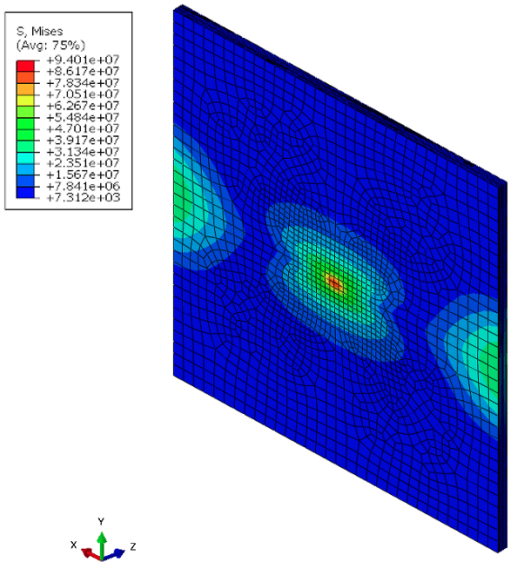

Figure 5.8: Stress distribution at the beginning of the analysis for initial impact energy of $8J$ (back view).

5.2 Results Comparison

In this section, a comparison between the experimental data from Sy *et al.* [62] and the numerical data obtained for this study is made. As a comparison, the work made by Sy *et al.* [66] where the effects of the twist angle on the material behaviour was not considered, was also included.

Initial Energy (J)	Absorbed Energy (J)			Difference from experimental (%)	
	Experimental Sy *et al.*	Numerical Sy *et al.*	Studied Model	Sy *et al.*	Studied Model
5	2,89	3,12	3,007	7,96	4,04
7	4,64	4,74	4,711	2,16	1,53
8	5,14	5,67	5,243	10,31	2,00
9	6,07	6,51	6,225	7,25	2,55
10	10	7,41	7,367	25,90	26,33

Table 5.3: Comparison between absorbed energy obtained using the model proposed in this study and the experimental results obtained by Sy *et al.* [62], and the numerical results obtained by Sy *et al.* [66]

From this comparison, it's possible to observe that the proposed model and numerical implementation poses a good prediction of a unidirectional flax fiber reinforced composites subjected to a low velocity

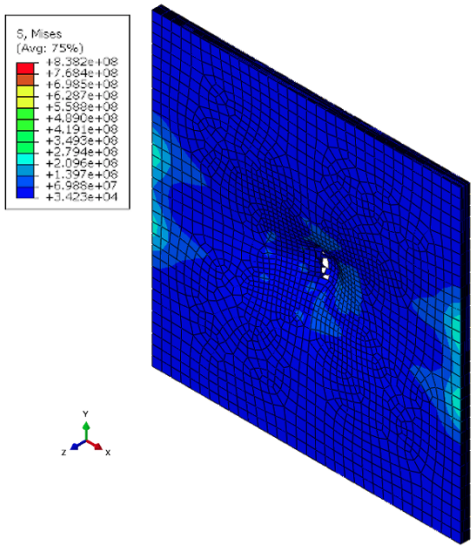

Figure 5.9: Stress distribution at the middle of the analysis for initial impact energy of 8J (front view).

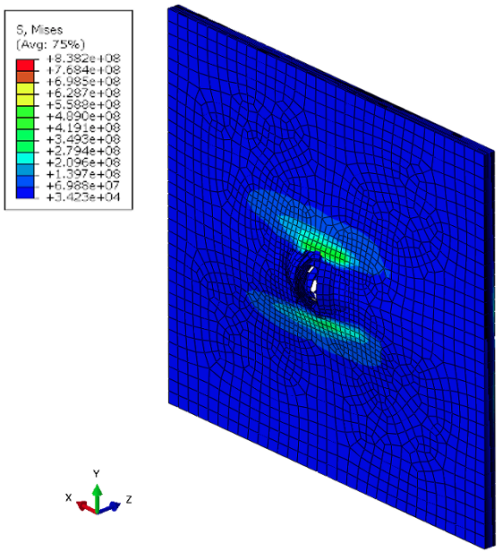

Figure 5.10: Stress distribution at the middle of the analysis for initial impact energy of 8J (back view).

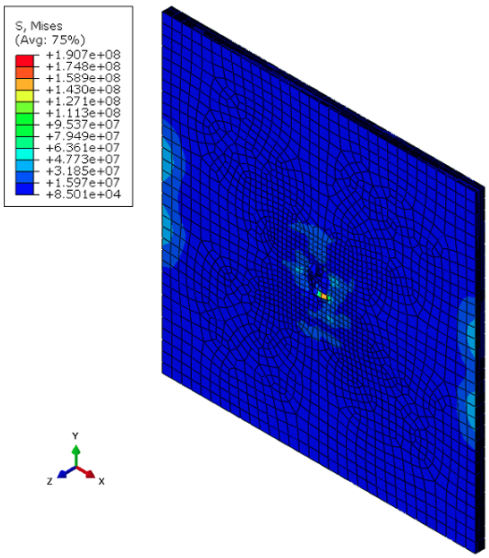

Figure 5.11: Stress distribution at the end of the analysis for initial impact energy of 8J (front view).

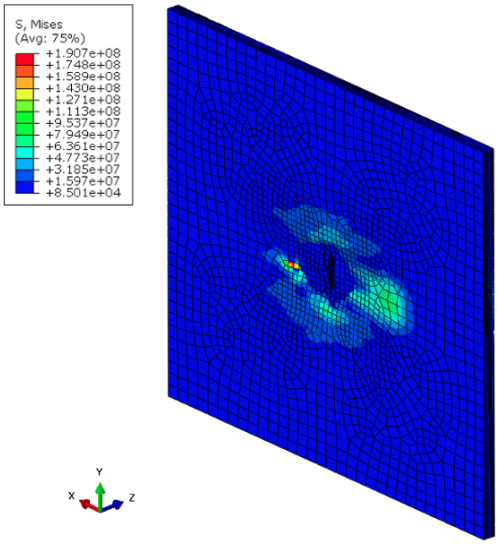

Figure 5.12: Stress distribution at the end of the analysis for initial impact energy of 8J (back view).

impact with energies up to 9 J. With the analysis made, the error was never superior to $\approx 4\%$ for the impact velocities of 5, 7, 8 and 9 J. The study for the energy of 10J was the one that presented the most deviation from the experimental results and this can be attributed to a difficulty to analyse and model the correct total failure behaviour of the material using the chosen criteria which does not take into consideration divisions of the failure modes like the example of delamination.

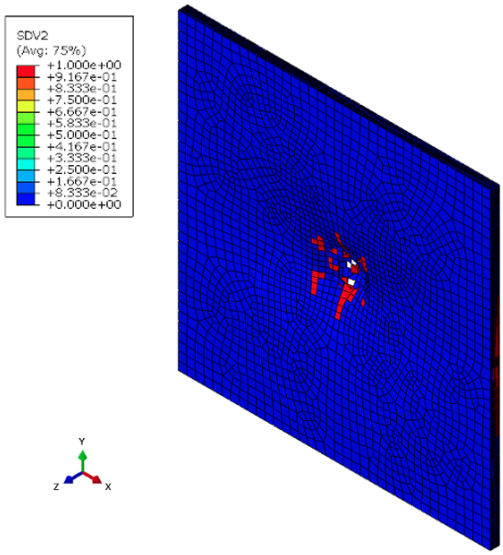

Figure 5.13: Fiber compressive damage at the middle of the analysis for initial impact energy of 8J (front view).

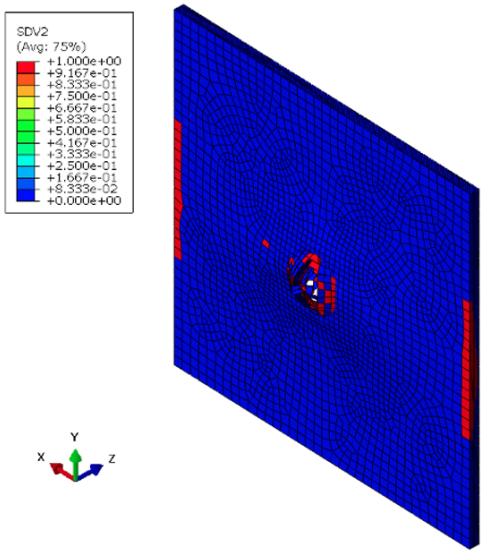

Figure 5.14: Fiber compressive damage at the middle of the analysis for initial impact energy of 8J(back view).

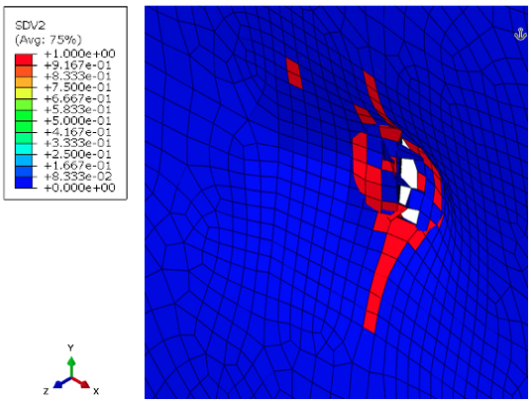

Figure 5.15: Detailed view of the fiber compressive damage at the middle of the analysis for initial impact energy of 8J (front view).

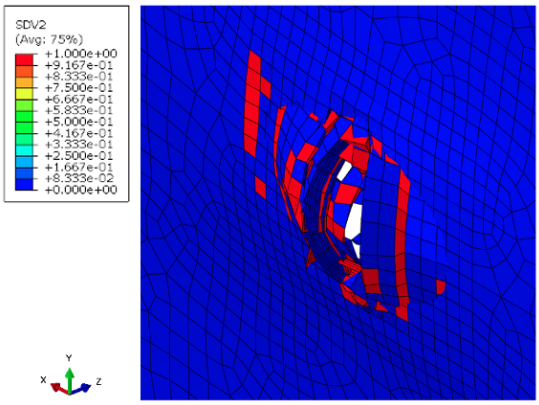

Figure 5.16: Detailed view of the fiber compressive damage at the middle of the analysis for initial impact energy of 8J(back view).

Even though the numerical results appear to present small differences when compared to the experimental results, the errors cannot be disregarded and there are some possible explanations for the difference in results. One of which is the manner that the composite was modelled without considering inter-ply interactions, that would have attributed to them an interaction property and would, possibly, predict a different behaviour of the relations between plies when under the impact load. Other relates to the approximations and assumptions made regarding the material properties for the application of a three dimensional criteria.

Comparing the results between the numerical results of Sy *et al.* [66] and the results from the numerical study made using the presented model, it is possible to verify some differences. The energy dissipation caused by the impact is better modelled by the implementation described with the dissipated energy

being still an over-estimation of the experimental results but being smaller in value, creating a smaller error. This might be a consequence of the assumptions made by Sy *et al.* [66] in their work that the material would have a linear behaviour. The present work considers the nonlinear behaviour caused by the twisting of the natural fibers and this might be an explanation for the improvement in the obtained results.

Chapter 6

Conclusions

The focus of the presented work was the development, implementation and validation of a constitutive model that would allow for a good analysis of unidirectional natural fiber yarn reinforced composites under a low velocity impact. The study and development of the model went through the considerations of various authors for the effects of the twist angle of the yarns reinforcing the fibers and possible implementations. The model then was chosen to be implemented using the Hashin failure criteria due to the possibility of the analysis of the progressive damage and after making the assumption of having a twisted yarn reduced to a plate under an off-axis stress state, it is necessary to also make the assumption that the presented model by Hashin for this (off-axis) case - where the ultimate tension for the fiber and matrix modes (σ_{fu}, σ_{mu}) - and found for the in-plane stress case, can be used on the three-dimensional case. Furthermore, it is necessary to consider the three-dimensional properties of the composite material to analyse it using the proposed model and, in a case such as the present one - where only properties for the in-plane case were available and there were no complete properties available for the constituent materials (epoxy and FlaxPly® UD-150) for the calculation of some properties (namely the properties that considered the third direction) - an approximation of these properties has to be made.

The implementation of the model, made using Abaqus/Explicit Finite Element Analysis software, was made using the user-defined subroutine VUMAT and required the use of Fortran programming language for the coding of the model using subroutines for the calculations needed in order to obtain the model implementation via VUMAT subroutine. It is also important to note that for an application like this, it is important to create a model using Abaqus/Explicit that will be used to input into the VUMAT subroutine linking them into a relation where the VUMAT has the model for the material behaviour and Abaqus/Explicit introduces into the VUMAT the material properties and parameters, gives the increments needed to the successive VUMAT iterations and also does the result post processing.

The author considers that the model and implementation presented in this study is a possible alternative for the study of a plant fiber (yarn) reinforced composite but recognizes that the analysis and validation of the model was limited to the data available on literature for low velocity impact on flax fiber reinforced composites and it is important to experimentally and numerically analyse and simulate cases with the same flax fiber reinforced composites but constituted by yarns with fibers spun in different

angle orientations in order to further validate the usefulness of the presented model and expand the scope of analysis to other natural sourced fiber spun into yarns, such as sisal or hemp. Nonetheless, the results obtained in the analysis performed were consistent to the literature available and showed a good estimation of the material behaviour when subjected to low velocity impact cases, except the case which the impact energy should cause catastrophic failure of the material which can be attributed to the non consideration of the inter-ply interactions.

6.1 Achievements

The present work's major achievement was the successful development and implementation of a viable model for the study of unidirectional plant fiber (more specifically flax fiber) reinforced composites when subjected to low velocity impacts. The successful validation of the presented and implemented model adds the possibility of using Abaqus/Explicit as a tool for the analysis of these materials which might incentive others to work on the subject, improve the models presented and develop better and more accurate investigation tools.

6.2 Future Work

For the future of the investigations on this subject, it would be advantageous to re-think and/or improve some aspects and simplifications of the presented model.

An interesting improvement to the model would be the introduction of the matrix failure modes from Puck into the matrix failure mode of the Hashin failure criteria, in order to better simulate the matrix failure and, possibly, improve the composite total failure.

The creation of a model of the composite plate that would include the inter-ply interactions introducing, for example, cohesive elements between plies. Since this type of study would increase the computational time, would also be interesting to investigate the possibility of extending the VUMAT subroutine to calculate the parameters needed to the utilization of shell elements on the simulation.

Other possible improvement would be the making of a mesh refinement study for each of the energy impact cases in order to find the optimal mesh refinement that would provide a good balance between computational time and results accuracy.

Bibliography

[1] S. Rana and R. Fangueiro, editors. *Advanced Composite Materials for Aerospace Engineering*. Woodhead Publishing, 2016. ISBN 978-0-08-100939-0.

[2] D. E. Airbus and F. A. Airbus. Special edition - a350xwb. *FAST (Flight Airworthiness Support Technology)*, Jun 2013.

[3] J. Bachmann, C. Hidalgo, and S. Bricout. Environmental analysis of innovative sustainable composites with potential use in aviation sector—a life cycle assessment review. *Science China Technological Sciences*, 60, 08 2017. doi: 10.1007/s11431-016-9094-y.

[4] Y. Li and B. Yuan. Nonlinear mechanical behavior of plant fiber reinforced composites. *Journal of Biobased Materials and Bioenergy*, 8, 04 2014. doi: 10.1166/jbmb.2014.1419.

[5] H. Ma, Y. Li, and D. Wang. Investigations of fiber twist on the mechanical properties of sisal fiber yarns and their composites. *Journal of Reinforced Plastics and Composites*, 33(7):687–696, 2014. doi: 10.1177/0731684413520187.

[6] H. Ma, Y. Li, Y. Shen, L. Xie, and D. Wang. Effect of linear density and yarn structure on the mechanical properties of ramie fiber yarn reinforced composites. *Composites Part A: Applied Science and Manufacturing*, 87:98 – 108, 2016. doi: https://doi.org/10.1016/j.compositesa.2016.04.012.

[7] J. Blanchard and A. Sobey. Comparative design of e-glass and flax structures based on reliability. *Composite Structures*, 225:111037, 2019. ISSN 0263-8223. doi: https://doi.org/10.1016/j.compstruct.2019.111037. URL `http://www.sciencedirect.com/science/article/pii/S0263822319306646`.

[8] P. Balakrishnan, M. John, L. Pothen, M. Sreekala, and S. Thomas. 12 - natural fibre and polymer matrix composites and their applications in aerospace engineering. In S. Rana and R. Fangueiro, editors, *Advanced Composite Materials for Aerospace Engineering*, pages 365–383. Woodhead Publishing, 2016. ISBN 978-0-08-100939-0. doi: https://doi.org/10.1016/B978-0-08-100037-3.00012-2.

[9] V. Sadrmanesh and Y. Chen. Bast fibres: structure, processing, properties, and applications. *International Materials Reviews*, 64(7):381–406, 2019. URL `https://doi.org/10.1080/09506608.2018.1501171`.

[10] M. Ramesh. Flax (linum usitatissimum l.) fibre reinforced polymer composite materials: A review

on preparation, properties and prospects. *Progress in Materials Science*, 102:109 – 166, 2019. ISSN 0079-6425. URL https://doi.org/10.1016/j.pmatsci.2018.12.004.

[11] M. Hubbe. Fibers. URL https://projects.ncsu.edu/project/hubbepaperchem/FIBR.htm.

[12] V. Sadrmanesh and Y. Chen. Bast fibres: structure, processing, properties, and applications. *International Materials Reviews*, 64(7):381–406, 2019. doi: 10.1080/09506608.2018.1501171.

[13] P. O. Sjoblom, J. T. Hartness, and T. M. Cordell. On low-velocity impact testing of composite materials. *Journal of Composite Materials*, 22(1):30–52, 1988. doi: 10.1177/002199838802200103.

[14] K. Shivakumar, W. Elber, and W. Illg. Prediction of low-velocity impact demage in thin circular laminates. *AIAA Journal*, 23, 04 1985. doi: 10.2514/3.8933.

[15] W. Cantwell and J. Morton. The impact resistance of composite materials — a review. *Composites*, 22(5):347 – 362, 1991. ISSN 0010-4361. doi: https://doi.org/10.1016/0010-4361(91)90549-V.

[16] S. Abrate. Impact on laminated composite materials. *Applied Mechanics Reviews - APPL MECH REV*, 44, 04 1991. doi: 10.1115/1.3119500.

[17] D. Liu and L. E. Malvern. Matrix cracking in impacted glass/epoxy plates. *Journal of Composite Materials*, 21(7):594–609, 1987. doi: 10.1177/002199838702100701.

[18] S. Joshi and C. Sun. Impact-induced fracture in quasi-isotropic laminate. 19, 02 1987. doi: 10.1520/CTR10427J.

[19] P. Robinson and G. Davies. Impactor mass and specimen geometry effects in low velocity impact of laminated composites. *International Journal of Impact Engineering*, 12:189–207, 12 1992. doi: 10.1016/0734-743X(92)90408-L.

[20] M. Richardson and M. Wisheart. Review of low-velocity impact properties of composite materials. *Composites Part A: Applied Science and Manufacturing*, 27(12):1123 – 1131, 1996. ISSN 1359-835X. doi: https://doi.org/10.1016/1359-835X(96)00074-7.

[21] J. N. Reddy. *Mechanics of laminated composite plates and shells : theory and analysis*. Boca Raton, Fla. ; London : CRC, 2nd ed edition, 2004. ISBN 0849315921.

[22] K. K. Chawla. *Fibrous materials*. Cambridge University Press, second edition, 2016. ISBN 9781139342520 (ebook).

[23] S. V. Hoa. *Principles of the Manufacturing of Composite Materials*. DEStech Publications, Inc., first edition, 2009. ISBN 978-1932078268.

[24] T. Keller, editor. *Advanced Composite Materials for Aerospace Engineering*. Zürich : International Association for Bridge and Structural Engineering, 2003. ISBN 3857481080 9783857481086.

[25] H. Ma, Y. Li, and D. Wang. Investigations of fiber twist on the mechanical properties of sisal fiber yarns and their composites. *Journal of Reinforced Plastics and Composites*, 33:687–696, 04 2014. doi: 10.1177/0731684413520187.

[26] V. Sadrmanesh and Y. Chen. Bast fibres: structure, processing, properties, and applications. *International Materials Reviews*, pages 1–26, 07 2018. doi: 10.1080/09506608.2018.1501171.

[27] E. McLaughlin and R. Tait. Fracture mechanism of plant fibres. *Journal of Materials Science*, 15 (1):89–95, 1980.

[28] D. Shah, P. Schubel, and M. Clifford. Modelling the effect of yarn twist on the tensile strength of unidirectional plant fibre yarn composites. *Journal of Composite Materials*, 47:425–436, 02 2013. doi: 10.1177/0021998312440737.

[29] J. Hearle, P. Grosberg, and S. Backer. *Structural Mechanics of Fibers, Yarns, and Fabrics*. Number vol. 1 in Structural Mechanics of Fibers, Yarns, and Fabrics. Wiley-Interscience, 1969. ISBN 9780471366690.

[30] K. Pickering, M. A. Efendy, and T. Le. A review of recent developments in natural fibre composites and their mechanical performance. *Composites Part A: Applied Science and Manufacturing*, 83:98 – 112, 2016. doi: https://doi.org/10.1016/j.compositesa.2015.08.038.

[31] Y. Shen, J. Zhong, S. Cai, H. Ma, Z. Qu, Y. Guo, and Y. Li. Effect of temperature and water absorption on low-velocity impact damage of composites with multi-layer structured flax fiber. *Materials*, 12:453, 02 2019. doi: 10.3390/ma12030453.

[32] Illinois department of public health - Fiberglass Fact Check. URL `http://www.idph.state.il.us/envhealth/factsheets/fiberglass.htm`.

[33] H. Alhashmy. Fabrication of aluminium matrix composites (amcs) by squeeze casting technique using carbon fiber as reinforcement. 10 2021.

[34] B. Harris et al. Engineering composite materials. 1999.

[35] M. Shioya, T. Itoh, T. Kunugi, and A. Takaku. Variation of longitudinal modulus with twist for yarns composed of high modulus fibers. *Textile Research Journal*, 71(10):928–936, 2001. doi: 10.1177/004051750107101013. URL `https://doi.org/10.1177/004051750107101013`.

[36] B. Madsen, P. Hoffmeyer, A. B. Thomsen, and H. Lilholt. Hemp yarn reinforced composites – i. yarn characteristics. *Composites Part A: Applied Science and Manufacturing*, 38(10):2194–2203, 2007. ISSN 1359-835X. doi: https://doi.org/10.1016/j.compositesa.2007.06.001. URL `https://www.sciencedirect.com/science/article/pii/S1359835X07001029`.

[37] N. Pan. Development of a constitutive theory for short fiber yams: Part iii: Effects of fiber orientation and bending deformation. *Textile Research Journal*, 63(10):565–572, 1993. doi: 10.1177/004051759306301002.

[38] P. Camanho. Failure criteria for fibre-reinforced polymer composites. 2002.

[39] S. W. Tsai and E. M. Wu. A general theory of strength for anisotropic materials. *Journal of Composite Materials*, 5(1):58–80, 1971. doi: 10.1177/002199837100500106.

[40] S. W. Tsai. Strength characteristics of composite materials. Technical report, Philco Corp Newport Beach CA, 1965.

[41] C. Chamis. Failure criteria for filamentary composites. In *Composite Materials: Testing and Design*. ASTM International, 1969.

[42] S. Joshi and C. Sun. Impact induced fracture in a laminated composite. *Journal of Composite Materials*, 19(1):51–66, 1985. doi: 10.1177/002199838501900104.

[43] S. Patil, M. Reddy D, and M. Reddy. Low velocity impact analysis on composite structures – a review. volume 1943, page 020009, 04 2018. doi: 10.1063/1.5029585.

[44] H. Y. Choi, R. J. Downs, and F.-K. Chang. A new approach toward understanding damage mechanisms and mechanics of laminated composites due to low-velocity impact: Part i—experiments. *Journal of Composite Materials*, 25(8):992–1011, 1991. doi: 10.1177/002199839102500803.

[45] C. Jih and C. Sun. Prediction of delamination in composite laminates subjected to low velocity impact. *Journal of Composite Materials*, 27(7):684–701, 1993. doi: 10.1177/002199839302700703.

[46] W. Cantwell and J. Morton. Geometrical effects in the low velocity response of cfrp. *Composite Structures*, 12:39–59, 01 2007. doi: 10.1016/0263-8223(89)90043-3.

[47] F.-K. Chang, H. Y. Choi, and S.-T. Jeng. Study on impact damage in laminated composites. *Mechanics of Materials*, 10(1):83 – 95, 1990. ISSN 0167-6636. doi: https://doi.org/10.1016/0167-6636(90)90019-C.

[48] G. Dorey. Impact damage in composites—development, consequences and prevention. In *Sixth International Conference on Composite Materials (and Second European Conference on Composite Materials)*, volume 3, 1987.

[49] D. Liu. Impact-induced delamination—a view of bending stiffness mismatching. *Journal of Composite Materials*, 22(7):674–692, 1988. doi: 10.1177/002199838802200706.

[50] M. LeBlanc and R. M. Measures. Impact damage assessment in composite materials with embedded fibre-optic sensors. *Composites Engineering*, 2(5):573 – 596, 1992. ISSN 0961-9526. doi: https://doi.org/10.1016/0961-9526(92)90044-7.

[51] G. Dorey, P. Sigety, K. Stellbrink, and W. Hart. Impact damage tolerance of carbon fibre and hybrid laminates. Technical report, ROYAL AIRCRAFT ESTABLISHMENT FARNBOROUGH (ENGLAND), 1987.

[52] A. Puck and H. Schürmann. Chapter 5.6 - failure analysis of frp laminates by means of physically based phenomenological models. In *Failure Criteria in Fibre-Reinforced-Polymer Composites*, pages 832–876. Elsevier, Oxford, 2004. doi: https://doi.org/10.1016/B978-008044475-8/50028-7.

[53] J. P. Boehler and M. Delafin. Failure criteria for unidirectional fiber-reinforced composites under confining pressure. In J.-P. Boehler, editor, *Mechanical Behavior of Anisotropic Solids / Comportment Méchanique des Solides Anisotropes*, pages 449–470, Dordrecht, 1982. Springer Netherlands. ISBN 978-94-009-6827-1.

[54] J. Mulhern, T. Rogers, and A. J. M. Spencer. A continuum model for fibre-reinforced plastic materials. *Proceedings of the Royal Society of London. Series A. Mathematical and Physical Sciences*, 301(1467):473–492, 1967.

[55] P. Linde, J. Pleitner, H. Boer, and C. Carmone. Modelling and simulation of fibre metal laminates. *ABAQUS Users' Conference*, 01 2004.

[56] J. Pederson. *Finite Element Analysis of Carbon FiberComposite Ripping Using ABAQUS*. PhD thesis, Clemson University, 2008.

[57] P. Liu, B. Liao, L. Jia, and X. Peng. Finite element analysis of dynamic progressive failure of carbon fiber composite laminates under low velocity impact. *Composite Structures*, 149:408–422, 2016. ISSN 0263-8223. doi: https://doi.org/10.1016/j.compstruct.2016.04.012.

[58] C. Zhang, E. A. Duodu, and J. Gu. Finite element modeling of damage development in cross-ply composite laminates subjected to low velocity impact. *Composite Structures*, 173:219–227, 2017. ISSN 0263-8223. doi: https://doi.org/10.1016/j.compstruct.2017.04.017.

[59] J. Zhou, P. Wen, and S. Wang. Finite element analysis of a modified progressive damage model for composite laminates under low-velocity impact. *Composite Structures*, 225:111113, 2019. ISSN 0263-8223. doi: https://doi.org/10.1016/j.compstruct.2019.111113.

[60] F. Wang, B. Wang, F. Kong, J. Ouyang, T. Ma, and Y. Chen. Assessment of degraded stiffness matrices for composite laminates under low-velocity impact based on modified characteristic length model. *Composite Structures*, 272:114145, 2021. ISSN 0263-8223. doi: https://doi.org/10.1016/j.compstruct.2021.114145. URL `https://www.sciencedirect.com/science/article/pii/S0263822321006073`.

[61] *Vumat*. Massachussets Institute of Technology - Abaqus Documentation. URL `https://abaqus-docs.mit.edu/2017/English/SIMACAESUBRefMap/simasub-c-vumat.htm`. Accessed on 2021/10/31.

[62] B. L. Sy, Z. Fawaz, and H. Bougherara. Damage evolution in unidirectional and cross-ply flax/epoxy laminates subjected to low velocity impact loading. *Composites Part A: Applied Science and Manufacturing*, 112:452–467, 2018. ISSN 1359-835X. doi: https://doi.org/10.1016/j.compositesa.2018.06.032.

[63] *Technical data sheet 2016: Flaxply UD 150*. Lineo, 2016. SANS LINEO, Saint Martin du Tilleul.

[64] Z. Mahboob, I. El Sawi, R. Zdero, Z. Fawaz, and H. Bougherara. Tensile and compressive damaged response in flax fibre reinforced epoxy composites. *Composites Part A: Applied Science and Manufacturing*, 92:118–133, 2017. ISSN 1359-835X. doi: https://doi.org/10.1016/j.compositesa.2016.11.007. URL `https://www.sciencedirect.com/science/article/pii/S1359835X16303785`.

[65] M. Z. Rahman. Mechanical and damping performances of flax fibre composites – a review. *Composites Part C: Open Access*, 4:100081, 2021. ISSN 2666-6820. doi: https://doi.org/10.1016/j.jcomc.2020.100081. URL `https://www.sciencedirect.com/science/article/pii/S2666682020300815`.

[66] B. L. Sy, Z. Fawaz, and H. Bougherara. Numerical simulation correlating the low velocity impact behaviour of flax/epoxy laminates. *Composites Part A: Applied Science and Manufacturing*, 126: 105582, 2019. ISSN 1359-835X. doi: https://doi.org/10.1016/j.compositesa.2019.105582.

[67] H. Y. Choi, R. J. Downs, and F.-K. Chang. A new approach toward understanding damage mechanisms and mechanics of laminated composites due to low-velocity impact: Part i—experiments. *Journal of Composite Materials*, 25(8):992–1011, 1991. doi: 10.1177/002199839102500803.

[68] Y. Li and B. Yuan. Nonlinear mechanical behavior of plant fiber reinforced composites. *Journal of Biobased Materials and Bioenergy*, 8, 04 2014. doi: 10.1166/jbmb.2014.1419.

Appendix A

VUMAT Subroutine

```
      Subroutine vumat(
c Read only -
     1  nblock, ndir, nshr, nstatev, nfieldv, nprops, lanneal,
     2  stepTime, totalTime, dt, cmname, coordMp, charLength,
     3  props, density, strainInc, relSpinInc,
     4  tempOld, stretchOld, defgradOld, fieldOld,
     5  stressOld, stateOld, enerInternOld, enerInelasOld,
     6  tempNew, stretchNew, defgradNew, fieldNew,
c Write only -
     7  stressNew, stateNew, enerInternNew, enerInelasNew )
c
      include 'vaba_param.inc'
c
      dimension props(nprops), density(nblock),
     1  coordMp(nblock,*),
     2  charLength(*), strainInc(nblock,ndir+nshr),
     3  relSpinInc(nblock,nshr), tempOld(nblock),
     4  stretchOld(nblock,ndir+nshr), defgradOld(nblock,ndir+nshr+nshr),
     5  fieldOld(nblock,nfieldv), stressOld(nblock,ndir+nshr),
     6  stateOld(nblock,nstatev), enerInternOld(nblock),
     7  enerInelasOld(nblock), tempNew(*),
     8  stretchNew(nblock,ndir+nshr), defgradNew(nblock,ndir+nshr+nshr),
     9  fieldNew(nblock,nfieldv), stressNew(nblock,ndir+nshr),
     1  stateNew(nblock,nstatev),
     2  enerInternNew(nblock), enerInelasNew(nblock)
*
      character*80 cmname
*
      parameter( zero = 0.d0, one = 1.d0, two = 2.d0, half = .5d0 )
*
      parameter(
     *     i_svd_DmgFiberT   = 1,
     *     i_svd_DmgFiberC   = 2,
     *     i_svd_DmgMatrixT  = 3,
     *     i_svd_DmgMatrixC  = 4,
     *     i_svd_statusMp   = 5,
     *     i_svd_dampStress = 6,
c     *     i_svd_dampStressXx = 6,
c     *     i_svd_dampStressYy = 7,
c     *     i_svd_dampStressZz = 8,
c     *     i_svd_dampStressXy = 9,
c     *     i_svd_dampStressYz = 10,
c     *     i_svd_dampStressZx = 11,
     *     i_svd_Strain   = 12,
c     *     i_svd_StrainXx = 12,
c     *     i_svd_StrainYy = 13,
c     *     i_svd_StrainZz = 14,
c     *     i_svd_StrainXy = 15,
c     *     i_svd_StrainYz = 16,
c     *     i_svd_StrainZx = 17,
     *     n_svd_required = 17 )
*
      parameter(
     *     i_s33_Xx = 1,
```

```
     *     i_s33_Yy = 2,
     *     i_s33_Zz = 3,
     *     i_s33_Xy = 4,
     *     i_s33_Yz = 5,
     *     i_s33_Zx = 6 )
*
* Structure of property array
      parameter (
     *     i_pro_E1    = 1,
     *     i_pro_E2    = 2,
     *     i_pro_E3    = 3,
     *     i_pro_nu12  = 4,
     *     i_pro_nu13  = 5,
     *     i_pro_nu23  = 6,
     *     i_pro_G12   = 7,
     *     i_pro_G13   = 8,
     *     i_pro_G23   = 9,
*
     *     i_pro_beta  = 19,
     *     i_pro_cost  = 20,
     *     i_pro_sint  = 21,
*
     *     i_pro_sigu1t = 10,
     *     i_pro_sigu1c = 11,
     *     i_pro_sigu2t = 12,
     *     i_pro_sigu2c = 13,
     *     i_pro_sigu3t = 14,
     *     i_pro_sigu3c = 15,
     *     i_pro_sigu12 = 16,
     *     i_pro_sigu13 = 17,
     *     i_pro_sigu23 = 18 )
* Temporary arrays
      dimension eigen(maxblk*3)
*
* Read material properties
*
      E1 = props(i_pro_E1)
      E2 = props(i_pro_E2)
      E3 = props(i_pro_E3)
      xnu12 = props(i_pro_nu12)
      xnu13 = props(i_pro_nu13)
      xnu23 = props(i_pro_nu23)
      G12 = props(i_pro_G12)
      G13 = props(i_pro_G13)
      G23 = props(i_pro_G23)
*
      xnu21 = xnu12 * E2 / E1
      xnu31 = xnu13 * E3 / E1
      xnu32 = xnu23 * E3 / E2
*
      cost = props(i_pro_cost)
      sint = props(i_pro_sint)
*
*
* Compute terms of stiffness matrix
      gg = one / ( one - xnu12*xnu21 - xnu23*xnu32 - xnu31*xnu13
     *     - two*xnu21*xnu32*xnu13 )
      C11  = E1 * ( one - xnu23*xnu32 ) * gg
      C22  = E2 * ( one - xnu13*xnu31 ) * gg
      C33  = E3 * ( one - xnu12*xnu21 ) * gg
      C12  = E1 * ( xnu21 + xnu31*xnu23 ) * gg
      C13  = E1 * ( xnu31 + xnu21*xnu32 ) * gg
      C23  = E2 * ( xnu32 + xnu12*xnu31 ) * gg
*
      f1t = props(i_pro_sigu1t)
      f1c = props(i_pro_sigu1c)
      f2t = props(i_pro_sigu2t)
      f2c = props(i_pro_sigu2c)
      f3t = props(i_pro_sigu3t)
      f3c = props(i_pro_sigu3c)
      f12 = props(i_pro_sigu12)
      f13 = props(i_pro_sigu13)
      f23 = props(i_pro_sigu23)
*
      beta = props(i_pro_beta)
*
* Assume purely elastic material at the beginning of the analysis
*
```

```
      if ( totalTime .eq. zero ) then
         if (nstatev .lt. n_svd_Required) then
            call xplb_abqerr(-2,'Subroutine VUMAT requires the'//
     *           'specification of %I state variables. Check the'//
     *           'definition of *DEPVAR in the input file.',
     *           n_svd_Required,zero,' ')
            call xplb_exit
         end if
         call OrthoEla3dExp ( nblock,
     *        stateOld(1,i_svd_DmgFiberT),
     *        stateOld(1,i_svd_DmgFiberC),
     *        stateOld(1,i_svd_DmgMatrixT),
     *        stateOld(1,i_svd_DmgMatrixC),
     *        C11, C22, C33, C12, C23, C13, G12, G23, G13,
     *        strainInc,
     *        stressNew )
         return
      end if
*
*  Update total elastic strain
      call strainUpdate ( nblock, strainInc,
     *     stateOld(1,i_svd_strain), stateNew(1,i_svd_strain) )
*
* Stress update
      call OrthoEla3dExp ( nblock,
     *     stateOld(1,i_svd_DmgFiberT),
     *     stateOld(1,i_svd_DmgFiberC),
     *     stateOld(1,i_svd_DmgMatrixT),
     *     stateOld(1,i_svd_DmgMatrixC),
     *     C11, C22, C33, C12, C23, C13, G12, G23, G13,
     *     stateNew(1,i_svd_strain),
     *     stressNew )
*
* Failure evaluation
*
      call copyr ( nblock,
     *     stateOld(1,i_svd_DmgFiberT), stateNew(1,i_svd_DmgFiberT) )
      call copyr ( nblock,
     *     stateOld(1,i_svd_DmgFiberC), stateNew(1,i_svd_DmgFiberC) )
      call copyr ( nblock,
     *     stateOld(1,i_svd_DmgMatrixT), stateNew(1,i_svd_DmgMatrixT) )
      call copyr ( nblock,
     *     stateOld(1,i_svd_DmgMatrixC), stateNew(1,i_svd_DmgMatrixC) )
      nDmg = 0
      call eig33Anal ( nblock, stretchNew, eigen )
      call Hashin3d  ( nblock, nDmg,
     *     f1t, f2t, f3t, f1c, f2c, f3c, f12, f23, f13, cost, sint,
     *     stateNew(1,i_svd_DmgFiberT),
     *     stateNew(1,i_svd_DmgFiberC),
     *     stateNew(1,i_svd_DmgMatrixT),
     *     stateNew(1,i_svd_DmgMatrixC),
     *     stateNew(1,i_svd_statusMp),
     *     stressNew, eigen )
*     -- Recompute stresses if new Damage is occurring
      if ( nDmg .gt. 0 ) then
         call OrthoEla3dExp ( nblock,
     *        stateNew(1,i_svd_DmgFiberT),
     *        stateNew(1,i_svd_DmgFiberC),
     *        stateNew(1,i_svd_DmgMatrixT),
     *        stateNew(1,i_svd_DmgMatrixC),
     *        C11, C22, C33, C12, C23, C13, G12, G23, G13,
     *        stateNew(1,i_svd_strain),
     *        stressNew )
      end if
*
* Beta damping
      if ( beta .gt. zero ) then
         call betaDamping3d ( nblock,
     *        beta, dt, strainInc,
     *        stressOld, stressNew,
     *        stateNew(1,i_svd_statusMp),
     *        stateOld(1,i_svd_dampStress),
     *        stateNew(1,i_svd_dampStress) )
      end if
*
* Integrate the internal specific energy (per unit mass)
*
```

```
      call EnergyInternal3d ( nblock, stressOld, stressNew,
     *   strainInc, density, enerInternOld, enerInternNew )
*
      return
      end

************************************************************
*   OrthoEla3dExp: Orthotropic elasticity - 3d             *
************************************************************
      subroutine OrthoEla3dExp ( nblock,
     *     dmgFiberT, dmgFiberC, dmgMatrixT, dmgMatrixC,
     *     C11, C22, C33, C12, C23, C13, G12, G23, G13,
     *     strain, stress )
*
      include 'vaba_param.inc'
*  Orthotropic elasticity, 3D case -
*
      parameter( zero = 0.d0, one = 1.d0, two = 2.d0)
      parameter(
     *     i_s33_Xx = 1,
     *     i_s33_Yy = 2,
     *     i_s33_Zz = 3,
     *     i_s33_Xy = 4,
     *     i_s33_Yz = 5,
     *     i_s33_Zx = 6,
     *     n_s33_Car = 6 )
*
      dimension  strain(nblock,n_s33_Car),
     *     dmgFiberT(nblock), dmgFiberC(nblock),
     *     dmgMatrixT(nblock), dmgMatrixC(nblock),
     *     stress(nblock,n_s33_Car)
*     -- shear fraction in matrix tension and compression mode
      parameter ( smt = 0.9d0, smc = 0.5d0 )
*
      do k = 1, nblock
*     -- Compute damaged stiffness
         dft = dmgFiberT(k)
         dfc = dmgFiberC(k)
         dmt = dmgMatrixT(k)
         dmc = dmgMatrixC(k)
         df = one - ( one - dft ) * ( one - dfc )
         dm = one - ( one - smt*dmt ) * ( one - smc*dmc)
*
         dC11 = ( one - df ) * C11
         dC22 = ( one - dm ) * C22
         dC33 = C33
         dC12 = ( one - df ) * ( one - dm ) * C12
         dC23 = ( one - dm ) * C23
         dC13 = ( one - df ) * C13
         dG12 = ( one - df ) * ( one - dm ) * G12
         dG23 = ( one - dm ) * G23
         dG13 = ( one - df ) * G13
*     -- Stress update
         stress(k,i_s33_Xx) = dC11 * strain(k,i_s33_Xx)
     *        + dC12 * strain(k,i_s33_Yy)
     *        + dC13 * strain(k,i_s33_Zz)
         stress(k,i_s33_Yy) = dC12 * strain(k,i_s33_Xx)
     *        + dC22 * strain(k,i_s33_Yy)
     *        + dC23 * strain(k,i_s33_Zz)
         stress(k,i_s33_Zz) = dC13 * strain(k,i_s33_Xx)
     *        + dC23 * strain(k,i_s33_Yy)
     *        + dC33 * strain(k,i_s33_Zz)
         stress(k,i_s33_Xy) = two * dG12 * strain(k,i_s33_Xy)
         stress(k,i_s33_Yz) = two * dG23 * strain(k,i_s33_Yz)
         stress(k,i_s33_Zx) = two * dG13 * strain(k,i_s33_Zx)
      end do
*
      return
      end

************************************************************
*   strainUpdate: Update total strain                      *
************************************************************
      subroutine strainUpdate ( nblock,
     *     strainInc, strainOld, strainNew )
*
      include 'vaba_param.inc'
*
```

```
      parameter(
     *     i_s33_Xx = 1,
     *     i_s33_Yy = 2,
     *     i_s33_Zz = 3,
     *     i_s33_Xy = 4,
     *     i_s33_Yz = 5,
     *     i_s33_Zx = 6,
     *     n_s33_Car = 6 )
*
      dimension strainInc(nblock,n_s33_Car),
     *     strainOld(nblock,n_s33_Car),
     *     strainNew(nblock,n_s33_Car)
*
      do k = 1, nblock
         strainNew(k,i_s33_Xx)= strainOld(k,i_s33_Xx)
     *                        + strainInc(k,i_s33_Xx)
         strainNew(k,i_s33_Yy)= strainOld(k,i_s33_Yy)
     *                        + strainInc(k,i_s33_Yy)
         strainNew(k,i_s33_Zz)= strainOld(k,i_s33_Zz)
     *                        + strainInc(k,i_s33_Zz)
         strainNew(k,i_s33_Xy)= strainOld(k,i_s33_Xy)
     *                        + strainInc(k,i_s33_Xy)
         strainNew(k,i_s33_Yz)= strainOld(k,i_s33_Yz)
     *                        + strainInc(k,i_s33_Yz)
         strainNew(k,i_s33_Zx)= strainOld(k,i_s33_Zx)
     *                        + strainInc(k,i_s33_Zx)
      end do
*
      return
      end

************************************************************
*   Hashin3d w/ Off-Axis Orientation: Evaluate Hashin 3d failure  *
*   criterion for fiber with twist                          *
************************************************************
      subroutine Hashin3d ( nblock, nDmg,
     *     f1t, f2t, f3t, f1c, f2c, f3c, f12, f23, f13, cost, sint,
     *     dmgFiberT, dmgFiberC, dmgMatrixT, dmgMatrixC,
     *     statusMp, stress, eigen )
*
      include 'vaba_param.inc'

      parameter( zero = 0.d0, one = 1.d0, half = 0.5d0, three =3.d0 )
      parameter(
     *     i_s33_Xx = 1,
     *     i_s33_Yy = 2,
     *     i_s33_Zz = 3,
     *     i_s33_Xy = 4,
     *     i_s33_Yz = 5,
     *     i_s33_Zx = 6,
     *     n_s33_Car = 6 )
*
      parameter(i_v3d_X=1,i_v3d_Y=2,i_v3d_Z=3 )
      parameter(n_v3d_Car=3 )
*
      parameter ( eMax = 1.00d0, eMin = -0.8d0 )
*
      dimension  dmgFiberT(nblock), dmgFiberC(nblock),
     *     dmgMatrixT(nblock), dmgMatrixC(nblock),
     *     stress(nblock,n_s33_Car),
     *     eigen(nblock,n_v3d_Car),
     *     statusMp(nblock)
*
      f1tInv = zero
      f2tInv = zero
      f3tInv = zero
      f1cInv = zero
      f2cInv = zero
      f3cInv = zero
      f12Inv = zero
      f23Inv = zero
      f13Inv = zero
*
      if ( f1t .gt. zero ) f1tInv = one / f1t
      if ( f2t .gt. zero ) f2tInv = one / f2t
      if ( f3t .gt. zero ) f3tInv = one / f3t
      if ( f1c .gt. zero ) f1cInv = one / f1c
      if ( f2c .gt. zero ) f2cInv = one / f2c
```

```
      if ( f3c .gt. zero ) f3cInv = one / f3c
      if ( f12 .gt. zero ) f12Inv = one / f12
      if ( f23 .gt. zero ) f23Inv = one / f23
      if ( f13 .gt. zero ) f13Inv = one / f13
*
      do k = 1, nblock
         if ( statusMp(k) .eq. one ) then
*
         lDmg = 0
*
         s11 = stress(k,i_s33_Xx)
         s22 = stress(k,i_s33_Yy)
         s33 = stress(k,i_s33_Zz)
         s12 = stress(k,i_s33_Xy)
         s23 = stress(k,i_s33_Yz)
         s13 = stress(k,i_s33_Zx)
*
*     Evaluate Fiber modes
         if ( s11 .gt. zero ) then
*     -- Tensile Fiber Mode
            rft = (s11*cost*((cost*f1tInv**2) + (sint*f12Inv**2)))**2
     *      + (s12*f12Inv )**2 + (s13*f13Inv )**2
            if ( rft .ge. one ) then
               lDmg = 1
               dmgFiberT(k) = one
            end if
         else if ( s11 .lt. zero ) then
*     -- Compressive Fiber Mode
            rfc = abs(s11) * f1cInv
            if ( rfc .ge. one ) then
               lDmg = 1
               dmgFiberC(k) = one
            end if
         end if
*
*     Evaluate Matrix Modes
            if ( ( s22 + s33 ) .gt. zero ) then
*     -- Tensile Matrix mode
            rmt=((s22+s33)*(sint*(sint*f2tInv**2) + (cost*f12Inv**2)))**2
     *       + (s23**2-s22*s33)*f23Inv**2
     *       + (s12**2+s13**2)*f12Inv**2
                  if ( rmt .ge. one ) then
                     lDmg = 1
                     dmgMatrixT(k) = one
                  end if
               else if ( ( s22 + s33 ) .lt. zero ) then
*     -- Compressive Matrix Mode
            rmc=(((f2c*half*f23Inv)**2)-1)*((s22+s33)*f2cInv)
     *       + ((s22+s33)*half*f23Inv)**2 + (s23**2-s22*s33)*f23Inv**2
     *       + (s12**2+s13**2)/f12Inv**2
                  if ( rmc .ge. one ) then
                     lDmg = 1
                     dmgMatrixC(k) = one
                  end if
               end if
*
         eigMax=max(eigen(k,i_v3d_X),eigen(k,i_v3d_Y),eigen(k,i_v3d_Z))
         eigMin=min(eigen(k,i_v3d_X),eigen(k,i_v3d_Y),eigen(k,i_v3d_Z))
         enomMax = eigMax - one
         enomMin = eigMin - one
*
         if ( enomMax .gt. eMax .or.
     *        enomMin .lt. eMin .or.
     *        dmgFiberT(k) .eq. one ) then
            statusMp(k) = zero
         end if
*
         nDmg = nDmk + lDmg
*
         end if
*
      end do
*
      return
      end

*************************************************************
*   betaDamping: Add beta damping                           *
```

```
*************************************************************
      subroutine betaDamping3d ( nblock,
     *     beta, dt, strainInc, sigOld, sigNew,
     *     statusMp, sigDampOld, sigDampNew )
*
      include 'vaba_param.inc'
*
      parameter(
     *     i_s33_Xx = 1,
     *     i_s33_Yy = 2,
     *     i_s33_Zz = 3,
     *     i_s33_Xy = 4,
     *     i_s33_Yz = 5,
     *     i_s33_Zx = 6,
     *     n_s33_Car = 6 )
*
      dimension  sigOld(nblock,n_s33_Car),
     *     sigNew(nblock,n_s33_Car),
     *     strainInc(nblock,n_s33_Car),
     *     statusMp(nblock),
     *     sigDampOld(nblock,n_s33_Car),
     *     sigDampNew(nblock,n_s33_Car)
*
      parameter ( zero = 0.d0, one = 1.d0, two=2.0d0,
     *     half = 0.5d0, third = 1.d0/3.d0 )
      parameter ( asmall = 1.d-16 )
*
      betaddt =  beta / dt
*
      do k =1 , nblock
         sigDampNew(k,i_s33_Xx) = betaddt * statusMp(k) *
     *        ( sigNew(k,i_s33_Xx)
     *        - ( sigOld(k,i_s33_Xx) - sigDampOld(k,i_s33_Xx) ) )
         sigDampNew(k,i_s33_Yy) = betaddt * statusMp(k) *
     *        ( sigNew(k,i_s33_Yy)
     *        - ( sigOld(k,i_s33_Yy) - sigDampOld(k,i_s33_Yy) ) )
         sigDampNew(k,i_s33_Zz) = betaddt * statusMp(k) *
     *        ( sigNew(k,i_s33_Zz)
     *        - ( sigOld(k,i_s33_Zz) - sigDampOld(k,i_s33_Zz) ) )
         sigDampNew(k,i_s33_Xy) = betaddt * statusMp(k) *
     *        ( sigNew(k,i_s33_Xy)
     *        - ( sigOld(k,i_s33_Xy) - sigDampOld(k,i_s33_Xy) ) )
         sigDampNew(k,i_s33_Yz) = betaddt * statusMp(k) *
     *        ( sigNew(k,i_s33_Yz)
     *        - ( sigOld(k,i_s33_Yz) - sigDampOld(k,i_s33_Yz) ) )
         sigDampNew(k,i_s33_Zx) = betaddt * statusMp(k) *
     *        ( sigNew(k,i_s33_Zx)
     *        - ( sigOld(k,i_s33_Zx) - sigDampOld(k,i_s33_Zx) ) )
*
         sigNew(k,i_s33_Xx) = sigNew(k,i_s33_Xx)+sigDampNew(k,i_s33_Xx)
         sigNew(k,i_s33_Yy) = sigNew(k,i_s33_Yy)+sigDampNew(k,i_s33_Yy)
         sigNew(k,i_s33_Zz) = sigNew(k,i_s33_Zz)+sigDampNew(k,i_s33_Zz)
         sigNew(k,i_s33_Xy) = sigNew(k,i_s33_Xy)+sigDampNew(k,i_s33_Xy)
         sigNew(k,i_s33_Yz) = sigNew(k,i_s33_Yz)+sigDampNew(k,i_s33_Yz)
         sigNew(k,i_s33_Zx) = sigNew(k,i_s33_Zx)+sigDampNew(k,i_s33_Zx)
*
      end do
*
      return
      end

*************************************************************
*   EnergyInternal3d: Compute internal energy for 3d case  *
*************************************************************
      subroutine EnergyInternal3d(nblock, sigOld, sigNew ,
     *   strainInc, curDensity, enerInternOld, enerInternNew)
*
      include 'vaba_param.inc'
*
      parameter(
     *     i_s33_Xx = 1,
     *     i_s33_Yy = 2,
     *     i_s33_Zz = 3,
     *     i_s33_Xy = 4,
     *     i_s33_Yz = 5,
     *     i_s33_Zx = 6,
     *     n_s33_Car = 6 )
*
```

```
      parameter( two = 2.d0, half = .5d0 )
*
      dimension sigOld (nblock,n_s33_Car), sigNew (nblock,n_s33_Car),
     *     strainInc (nblock,n_s33_Car), curDensity (nblock),
     *     enerInternOld(nblock), enerInternNew(nblock)
*
      do k = 1, nblock
         stressPower  = half * (
     *        ( sigOld(k,i_s33_Xx) + sigNew(k,i_s33_Xx) )
     *        * ( strainInc(k,i_s33_Xx) )
     *        +       ( sigOld(k,i_s33_Yy) + sigNew(k,i_s33_Yy) )
     *        * ( strainInc(k,i_s33_Yy))
     *        +       ( sigOld(k,i_s33_Zz) + sigNew(k,i_s33_Zz) )
     *        * ( strainInc(k,i_s33_Zz))
     *        + two * ( sigOld(k,i_s33_Xy) + sigNew(k,i_s33_Xy) )
     *        * strainInc(k,i_s33_Xy)
     *        + two * ( sigOld(k,i_s33_Yz) + sigNew(k,i_s33_Yz) )
     *        * strainInc(k,i_s33_Yz)
     *        + two * ( sigOld(k,i_s33_Zx) + sigNew(k,i_s33_Zx) )
     *        * strainInc(k,i_s33_Zx) )
*
         enerInternNew(k) = enerInternOld(k) + stressPower/curDensity(k)
      end do
*
      return
      end

************************************************************
*   CopyR: Copy from one array to another                  *
************************************************************
      subroutine CopyR(nCopy, from, to )
*
      include 'vaba_param.inc'
*
      dimension from(nCopy), to(nCopy)
*
      do k = 1, nCopy
         to(k) = from(k)
      end do
*
      return
      end

************************************************************************
*****
* eig33Anal: Compute eigen values of a 3x3 symmetric matrix analytically *
************************************************************************
*****
      subroutine eig33Anal( nblock, sMat, eigVal )
*
      include 'vaba_param.inc'
*
      parameter(i_s33_Xx=1,i_s33_Yy=2,i_s33_Zz=3 )
      parameter(i_s33_Xy=4,i_s33_Yz=5,i_s33_Zx=6 )
      parameter(i_s33_Yx=i_s33_Xy )
      parameter(i_s33_Zy=i_s33_Yz )
      parameter(i_s33_Xz=i_s33_Zx,n_s33_Car=6 )
*
      parameter(i_v3d_X=1,i_v3d_Y=2,i_v3d_Z=3 )
      parameter(n_v3d_Car=3 )
*
      parameter ( zero = 0.d0, one = 1.d0, two = 2.d0,
     *     three = 3.d0, half = 0.5d0, third = one / three,
     *     pi23 = 2.094395102393195d0,
     *     fuzz = 1.d-8,
     *     preciz = fuzz * 1.d4 )
*
      dimension eigVal(nblock,n_v3d_Car), sMat(nblock,n_s33_Car)
*
      do k = 1, nblock
        sh  = third*(sMat(k,i_s33_Xx)+sMat(k,i_s33_Yy)+sMat(k,i_s33_Zz))
        s11 = sMat(k,i_s33_Xx) - sh
        s22 = sMat(k,i_s33_Yy) - sh
        s33 = sMat(k,i_s33_Zz) - sh
        s12 = sMat(k,i_s33_Xy)
        s13 = sMat(k,i_s33_Xz)
        s23 = sMat(k,i_s33_Yz)
*
        fac  = max(abs(s11), abs(s22), abs(s33))
        facs = max(abs(s12), abs(s13), abs(s23))
        if( facs .lt. (preciz*fac) ) then
```

```
            eigVal(k,i_v3d_X) = sMat(k,i_s33_Xx)
            eigVal(k,i_v3d_Y) = sMat(k,i_s33_Yy)
            eigVal(k,i_v3d_Z) = sMat(k,i_s33_Zz)
          else
            q = third*((s12**2+s13**2+s23**2)+half*(s11**2+s22**2+s33**2))
            fac = two * sqrt(q)
            if( fac .gt. fuzz ) then
              ofac = two/fac
            else
              ofac = zero
            end if
            s11 = ofac*s11
            s22 = ofac*s22
            s33 = ofac*s33
            s12 = ofac*s12
            s13 = ofac*s13
            s23 = ofac*s23
            r = s12*s13*s23
     *          + half*(s11*s22*s33-s11*s23**2-s22*s13**2-s33*s12**2)
            if( r .ge. one-fuzz ) then
              cos1 = -half
              cos2 = -half
              cos3 = one
            else if( r .le. fuzz-one ) then
              cos1 = -one
              cos2 = half
              cos3 = half
            else
              ang = third * acos(r)
              cos1 = cos(ang)
              cos2 = cos(ang+pi23)
              cos3 =-cos1-cos2
            end if
            eigVal(k,i_v3d_X) = sh + fac*cos1
            eigVal(k,i_v3d_Y) = sh + fac*cos2
            eigVal(k,i_v3d_Z) = sh + fac*cos3
          end if
        end do
*
        return
        end
```

Appendix B

VUMAT Variables

Basic variables for the VUMAT user defined subroutine, according to [61].

• ***Variables that can be defined***

stressNew (nblock, ndir+nshr) Stress tensor at each material point at the end of the increment.

stateNew (nblock, nstatev) State variables at each material point at the end of the increment.

• ***Variables that can be updated***

enerInternNew (nblock) Internal energy per unit mass at each material point at the end of the increment.

enerInelasNew (nblock) Dissipated inelastic energy per unit mass at each material point at the end of the increment.

• ***Variables passed in for information***

nblock Number of material points to be processed in this call to VUMAT.

ndir Number of direct components in a symmetric tensor.

nshr Number of indirect components in a symmetric tensor.

nstatev Number of user-defined state variables that are associated with this material type (you define this as described in Allocating space).

nfieldv Number of user-defined external field variables.

nprops User-specified number of user-defined material properties.

lanneal Flag indicating whether the routine is being called during an annealing process. lanneal=0 indicates that the routine is being called during a normal mechanics increment. lanneal=1 indicates that this is an annealing process and you should re-initialize the internal state variables, stateNew, if necessary. Abaqus/Explicit will automatically set the stresses, stretches, and state to a value of zero during the annealing process.

stepTime Value of time since the step began.

totalTime Value of total time. The time at the beginning of the step is given by totalTime - stepTime.

dt Time increment size.

cmname User-specified material name, left justified. It is passed in as an uppercase character string. Some internal material models are given names starting with the "ABQ " character string. To avoid conflict, you should not use "ABQ " as the leading string for cmname.

coordMp(nblock,*) Material point coordinates. It is the midplane material point for shell elements and the centroid for beam and pipe elements.

charLength(nblock) Characteristic element length, which is either the default value based on the geometric mean or the user-defined characteristic element length defined in user subroutine VUCHARLENGTH. The default value is a typical length of a line across an element for a first-order element; it is half of the same typical length for a second-order element. For beams, pipes, and trusses, the default value is a characteristic length along the element axis. For membranes and shells it is a characteristic length in the reference surface. For axisymmetric elements it is a characteristic length in the r–z plane only. For cohesive elements it is equal to the constitutive thickness.

props(nprops) User-supplied material properties.

density(nblock) Current density at the material points in the midstep configuration. This value may be inaccurate in problems where the volumetric strain increment is very small. If an accurate value of the density is required in such cases, the analysis should be run in double precision. This value of the density is not affected by mass scaling.

strainInc (nblock, ndir+nshr) Strain increment tensor at each material point.

relSpinInc (nblock, nshr) Incremental relative rotation vector at each material point defined in the corotational system. Defined as $\Delta t(W - \Omega$, where W is the antisymmetric part of the velocity gradient, L, and$\Omega = \dot{R} \cdot R^T$. Stored in 3D as (32,13,21) and in 2D as (21).

tempOld(nblock) Temperatures at each material point at the beginning of the increment.

stretchOld (nblock, ndir+nshr) Stretch tensor, U, at each material point at the beginning of the increment defined from the polar decomposition of the deformation gradient by $F = R \cdot U$.

defgradOld (nblock,ndir+2*nshr) Deformation gradient tensor at each material point at the beginning of the increment. Stored in 3D as $(F_{11}, F_{22}, F_{33}, F_{12}, F_{23}, F_{31}, F_{21}, F_{32}, F_{13})$ and in 2D as $(F_{11}, F_{22}, F_{33}, F_{12}, F_{21})$.

fieldOld (nblock, nfieldv) Values of the user-defined field variables at each material point at the beginning of the increment.

stressOld (nblock, ndir+nshr) Stress tensor at each material point at the beginning of the increment.

stateOld (nblock, nstatev) State variables at each material point at the beginning of the increment.

enerInternOld (nblock) Internal energy per unit mass at each material point at the beginning of the increment.

enerInelasOld (nblock) Dissipated inelastic energy per unit mass at each material point at the beginning of the increment.

tempNew(nblock) Temperatures at each material point at the end of the increment.

stretchNew (nblock, ndir+nshr) Stretch tensor, U, at each material point at the end of the increment defined from the polar decomposition of the deformation gradient by $F = R \cdot U$.

defgradNew (nblock,ndir+2*nshr) Deformation gradient tensor at each material point at the end of the increment. Stored in 3D as $(F_{11}, F_{22}, F_{33}, F_{12}, F_{23}, F_{31}, F_{21}, F_{32}, F_{13})$ and in 2D as $(F_{11}, F_{22}, F_{33}, F_{12}, F_{21})$.

fieldNew (nblock, nfieldv) Values of the user-defined field variables at each material point at the end of the increment.